



Identification of new highly selective inhibitors of the human ADP/ATP carriers by molecular docking and *in vitro* transport assays



Simona Todisco^{a,b,1}, Maria Antonietta Di Noia^{a,1}, Angelo Onofrio^{a,1}, Giovanni Parisi^{a,1}, Giuseppe Punzi^{a,1}, Giandomenico Redavid^a, Anna De Grassi^a, Ciro Leonardo Pierri^{a,*}

^a Department of Biosciences, Biotechnologies and Biopharmaceutics, University of Bari, Via Orabona 4, 70125 Bari, Italy

^b Department of Sciences, University of Basilicata, Via N. Sauro 85, 85100 Potenza, Italy

ARTICLE INFO

Article history:

Received 7 October 2015

Accepted 18 November 2015

Available online 23 November 2015

Chemical compounds studied in this article:

Carboxyatractyloside (PubChem CID: 75069414)

Bongkrekkic acid (PubChem CID: 6433556)

Steviol (PubChem CID: 9905087)

Suramin (PubChem CID: 5361)

Chebulinic acid (PubChem CID: 72284)

Saikosaponin (PubChem CID: 441945)

Keywords:

Mitochondrial carriers

ADP/ATP carrier inhibitors

Apoptosis inducers

IC50

K_i

Docking-based virtual screening of chemical libraries

Suramin

Chebulinic acid

Carboxyatractyloside

Bongkrekkic acid

ABSTRACT

Mitochondrial carriers are proteins that shuttle a variety of metabolites, nucleotides and coenzymes across the inner mitochondrial membrane. The mitochondrial ADP/ATP carriers (AACs) specifically translocate the ATP synthesized within mitochondria to the cytosol in exchange for the cytosolic ADP, playing a key role in energy production, in promoting cell viability and regulating mitochondrial permeability transition pore opening. In *Homo sapiens* four genes code for AACs with different tissue distribution and expression patterns. Since AACs are dysregulated in several cancer types, the employment of known and new AAC inhibitors might be crucial for inducing mitochondrial-mediated apoptosis in cancer cells. Albeit carboxyatractyloside (CATR) and bongkrekkic acid (BKA) are known to be powerful and highly selective AAC inhibitors, able to induce mitochondrial dysfunction at molecular level and poisoning at physiological level, we estimated here for the first time their affinity for the human recombinant AAC2 by *in vitro* transport assays. We found that the inhibition constants of CATR and BKA are 4 nM and 2.0 μ M, respectively. For finding new AAC inhibitors we also performed a docking-based virtual screening of an in-house developed chemical library and we identified about 100 ligands showing high affinity for the AAC2 binding region. By testing 13 commercially available molecules, out of the 100 predicted candidates, we found that 2 of them, namely suramin and chebulinic acid, are competitive AAC2 inhibitors with inhibition constants 0.3 μ M and 2.1 μ M, respectively. We also demonstrated that chebulinic acid and suramin are “highly selective” AAC2 inhibitors, since they poorly inhibit other human mitochondrial carriers (namely ORC1, APC1 and AGC1).

© 2015 Elsevier Inc. All rights reserved.

1. Introduction

ADP/ATP carriers (AACs) are protein members of the mitochondrial carrier family (SLC25A family [1–3]) and they supply the ATP synthesized within mitochondria to the cytosol in exchange for the

cytosolic ADP [4]. Due to their involvement in the regulation of cell viability [3,5,6] and apoptosis triggering [7–9] AACs are among the most studied mitochondrial carriers (MCs). Four genes coding for AACs have been found in *Homo sapiens*, namely SLC25A4, SLC25A5, SLC25A6 and SLC25A31. Each AAC gene has a tissue-specific expression pattern, which is similar in different mammals, and may be related to developmental stage, status of cell proliferation and tissue-specific energy requirements. For example, AAC1 (encoded by SLC25A4) is highly expressed in terminally differentiated tissues such as skeletal muscles, heart and brain, AAC3 (encoded by SLC25A6) is ubiquitously expressed in all tissues, whereas AAC4 (encoded by SLC25A31) is a murine stem and germ-cell isoform [10–12]. Notably, AAC2 (encoded by SLC25A5) is specifically expressed in undifferentiated cells, such as lymphocytes, or in tissues that are able to proliferate and regenerate, such as those of the kidney and liver [10,13].

Abbreviations: AACs, human ADP/ATP carriers; AAC2, ADP/ATP carrier paralog 2; AGC1, aspartate/glutamate carrier paralog 1; APC1, ATP-Mg/Pi carrier paralog 1; ATR, atractyloside; BKA, bongkrekkic acid; CATR, carboxyatractyloside; MCs, mitochondrial carriers; ORC1, ornithine carrier paralog 1; Pi, phosphate; PTP, permeability transition pore; STE, steviol; STD, stevioside.

* Corresponding author: Ciro Leonardo Pierri, Department of Biosciences, Biotechnologies and Biopharmaceutics, University of Bari, via Orabona, 4, 70125, Bari, Italy. Tel.: +39 0805443614; fax: +39 0805442770.

E-mail addresses: ciroleopierri@gmail.com, ciro.pierri@uniba.it (C.L. Pierri).

¹ These authors contributed equally to this work.

At variance with AAC1 and AAC3, the expression of AAC2 was recently found upregulated in several hormone-dependent cancers [14]. This induction of AAC2 expression in cancer cells was directly associated to glycolytic metabolism raising a question regarding the role of AAC2 during carcinogenesis [15–17]. It was also reported that the AAC2 knocking down/silencing [14,18] leads to cell growth/proliferation arrest and in combination with other treatments decreases cancer cell resistance to traditional therapies [19,20]. The above reported findings imply that AAC2 inhibits or negatively modulates the opening of the mitochondrial membrane permeability transition pore (PTP) [7–9] acting as an antiapoptotic protein [21].

It is also known that two ligands, carboxyatractyloside (CATR) and bongkreikic acid (BKA), are powerful and highly selective inhibitors of the mitochondrial AACs [4]. CATR is a diterpenoid glycoside isolated from Cocklebur seeds (from *Xanthium strumarium*) [22], whereas BKA is a natural toxin isolated from the bacterium *Burkholderia cocovenenans* [23]. It is worth noting that the CATR interacts directly with AACs proposed binding region [24], thus inhibiting AACs from the cytosolic face, whereas BKA is able to inhibit AACs from the matrix side [25]. It was noticed that the inhibition of AACs through atractyloside (ATR), which corresponds to the decarboxylated CATR, caused poisoning at physiological level [26–28]. Furthermore, it has been reported that the consumption of plants containing ATR or CATR caused fatal renal proximal tubule necrosis and/or centrilobular hepatic necrosis in man and farm animals [29].

In addition to CATR and BKA, other molecules were proposed to inhibit adenine nucleotides translocation from mitochondria to the cytosol and *vice versa*, however nobody estimated their inhibition constants (K_i), or their affinity for recombinant AACs. The first molecule is stevioside (STD, structurally related to CATR), which is a traditional remedy against diabetes and a world widely used sweetener, isolated from *Stevia rebaudiana*. The second molecule is steviol (STE), which is the aglycosylated metabolite of stevioside. Those molecules were proposed to be AAC inhibitors based on their ability in inhibiting ATP synthesis in rat liver mitochondria [30] or ATP uptake in bovin mitochondria or isolated AAC proteins from bovin mitochondria [31,32]. For the first time, here we estimated the affinity of old and newly proposed inhibitors for AACs by transport assays on the human recombinant AAC2. With this purpose, we firstly have overexpressed in *Escherichia coli* the human AAC2 gene as recombinant protein and then we estimated the K_i of CATR and BKA for AAC2 by transport assays [33–35]. We have confirmed that AAC2 is inhibited by CATR and BKA at very low concentrations. Furthermore, by performing a docking-based virtual-screening of an in-house developed chemical library, we have predicted novel AAC inhibitors and assayed their effect on the transport activity of the human recombinant AAC2, finding that two of them, *i.e.* suramin and chebulinic acid, are new highly selective AAC inhibitors.

2. Materials and methods

2.1. Materials

Radioactive compounds were supplied from PerkinElmer Life Sciences. All nucleotides, deoxynucleotides and the tested inhibitors were purchased from Sigma.

2.2. Construction of an expression plasmid for AAC2

Primers for amplifying SLC25A5_AAC2 (NP_001143.2) were designed based on mRNA sequences (NM_001152.4). Two primer pairs were used to amplify cDNA first strand obtained from human B-lymphocytes with a nested PCR. The first primer pair was

designed at 5' and 3' UTR of SLC25A5_AAC2 gene. The second primer pair was designed based on the start and stop codon with additional NdeI and XhoI restriction sites as linkers at 5' end allowing unidirectional cloning (Table 1). The amplified product was digested (NdeI/XhoI) and cloned into pET21b vector (Life Technologies) for expression in *E. coli*. The plasmid containing the sequence coding for AAC2 was transformed into *E. coli* TG1 competent cells. Transformants were selected on LB plates containing ampicillin (100 µg/ml) and screened by direct colony PCR and by restriction digestion of purified plasmids. The sequence of the insert was verified by DNA sequencing (StarSEQ).

2.3. Bacterial expression and purification of recombinant AAC2

The expression of the recombinant AAC2 was obtained after 4 h induction with isopropyl β-D-1-thiogalactopyranoside (IPTG, final concentration 0.7 mM added after cell O.D. = 0.4 – 0–6) carried out at 37 °C in *E. coli* BL21(DE3) strain [35–37] according to the manufacturer's instructions. Control cultures with the empty vector were processed in parallel. Inclusion bodies were purified on a sucrose density gradient [36,37] and washed at 4 °C first with TE buffer (10 mM Tris/HCl, 1 mM EDTA, pH 7.0), then with a TNS buffer (Triton X-114 (3% w/v), 20 mM sodium sulfate, 1 mM EDTA and 10 mM PIPES/NaOH (pH 7.0)). Finally, the obtained inclusion bodies were washed again using TE buffer.

2.4. Reconstitution of AAC2 into liposomes

The AAC2 recombinant protein was solubilized in 1.2% (w/v) sarkosyl (*N*-lauroylsarcosine sodium salt) and reconstituted into liposomes by cyclic removal of the detergent with a hydrophobic column of Amberlite beads (Fluka), as previously described [34], with some modifications. The composition of the initial mixture used for reconstitution was 10 µl of solubilized AAC2 (20 µg of protein), 70 µl of 10% Triton X-114, 100 µl of 10% phospholipids (L-α-phosphatidylcholine from egg yolk from Sigma) in the form of sonicated liposomes, 10 mM substrate except where otherwise indicated, 0.7 mg of cardiolipin, 10 mM PIPES-NaOH (pH 7.0) and water to a final volume of 700 µl. After vortexing, this mixture was recycled 13-times through an Amberlite column (3.2 × 0.5 cm) pre-equilibrated with a buffer containing 10 mM PIPES-NaOH (pH 7.0). All operations were performed at 4 °C except for the passages through Amberlite, which were carried out at room temperature.

2.5. Transport measurements

External substrate was removed from proteoliposomes on Sephadex G-75 columns pre-equilibrated with 50 mM NaCl and 10 mM PIPES-NaOH at pH 7.0 (buffer A). The eluted proteoliposomes were distributed in reaction vessels, then transport was started at 25 °C by adding externally [³H]ATP or [¹⁴C]ADP to substrate-loaded proteoliposomes (exchange) or to NaCl loaded proteoliposomes (uniport). In both cases, transport was stopped by adding 30 mM pyridoxal-5'-phosphate and 20 mM bathophenanthroline, which in combination and at high concentrations inhibit the activity of several mitochondrial carriers rapidly and completely [37–40]. In controls, the inhibitors were added at

Table 1
Primers for AAC2 amplification.

Primer	Sequence (5'-3')
AAC2For1	cctataaatcgccattgtcttc
AAC2Rev1	cccatcatcatcatggaatg
AAC2For2	agggtaccatgatgACAGATGCCCTGTGTCCTTC
AAC2Rev2	gctaagtctcgagTTATGTGTACTTCTTGATTTCATACAAAG

the beginning together with the radioactive substrate. Finally, the external radiolabeled substrates was removed from each sample of proteoliposomes by a Sephadex G-75 column pre-equilibrated with buffer A and the radioactivity entrapped within proteoliposomes was measured. The experimental values were corrected by subtracting control values. The initial transport rate was calculated from the radioactivity taken up by proteoliposomes after 30 s (in the initial linear range of substrate uptake).

2.6. Inhibition assays

Transport measurements were also performed in presence of different concentrations of the investigated inhibitors, added simultaneously with the radiolabeled substrates. The percentage of residual transport activity was graphed against the corresponding \log_{10} inhibitor concentration in order to determine IC50 values of the tested inhibitors, namely the inhibitor concentration that caused a 50% reduction of the maximum transport activity. Although IC50 is not a direct estimation of inhibitor affinity for AAC2, IC50 and inhibitor affinity can be related through the following Cheng–Prusoff Eqs. (1) and (2) [41]:

$$IC50 = K_i \times \left(1 + \frac{[S]}{K_m}\right); \text{ for competitive inhibitors} \quad (1)$$

$$IC50 \simeq K_i; \quad \text{for non competitive inhibitors} \quad (2)$$

Furthermore, primary Lineweaver–Burk plots (namely double reciprocal plots) were used for determining the K_m of ATP and ADP for AAC2 and for investigating inhibition mechanisms according to Eqs. (3) (in absence of inhibitors), (4) and (5) (describing enzyme activity in presence of competitive or pure non-competitive inhibitors, respectively):

$$\frac{1}{V} = \frac{K_m}{V_{\max} \times [S]} + \frac{1}{V_{\max}}; \quad \text{without inhibitors} \quad (3)$$

$$\frac{1}{V} = \frac{K_m \times (1 + [I]/K_i)}{V_{\max} \times [S]} + \frac{1}{V_{\max}}; \quad \text{for competitive inhibitors} \quad (4)$$

$$\frac{1}{V} = \frac{K_m \times (1 + [I]/K_i)}{V_{\max} \times [S]} + \frac{(1 + [I]/K_i)}{V_{\max}}; \quad \text{for pure non – competitive inhibitors} \quad (5)$$

where “V” represents the initial rate in the presence of the only substrate ([S]) or of substrate and inhibitor ([I]). K_m is the Michaelis–Menten constant (namely half-saturation constant), K_i is the inhibition constant. Finally, secondary plots of the slopes of the double reciprocal plots [42] against inhibitor concentration (for each analyzed inhibitor) were used for calculating K_i values for the assayed competitive and non competitive inhibitors. The K_i obtained from secondary plots were in agreement with K_i obtained according the above reported equations.

2.7. Comparative modeling and virtual screening of a chemical library

The comparative 3D structural model of the SLC25A5_AAC2 protein was prepared by using Modeller [43]. The 3D BtAAC1 structure (PDB_ID: 1okc.pdb) was used as a protein template for building the human AAC2 3D model, sharing more than 89% of identical residues with it. The 3D modeling was performed according to our validated protocols [44,45].

The chemical library used for our docking-based virtual screening was created by taking all the ligands greater than 10 atoms and lighter than 1200 g/mol from the KEGG ligand database [46]. Ligands containing heavy metals were removed from the extracted library. All the ligands were in “.mol2” format. Notably, we added to this library the known AAC inhibitors such as CATR (taken from the crystallized BtAAC1 structure), ATR, BKA, and STE (taken from the pubchem database [47]) as reference inhibitors [4,24,30]. It should be stressed that in our library we used both the α - and β -D-glucosides for CATR. All the cited ligands were converted in “.mol2” files by using OpenBabel (http://openbabel.org/wiki/Main_Page) [48]. We also ascertained that in the selected ligand library ATP, ADP, AMP and the corresponding deoxynucleotides were present to be used as reference substrates. All the ligand structures within our library were energetically optimized (2D ligands were converted in 3D ligands, missing hydrogen atoms and charges were added where necessary) by using DG-AMMOS (Distance Geometry and Automatic Molecular Mechanics Optimization for *in silico* Screening, <http://www.mti.univ-paris-diderot.fr/fr/downloads.html>) [49]. The obtained library counted for 6492 unique ligands.

Before proceeding with the docking runs, the AAC2 3D model was prepared for the docking simulation converting the AAC2 “.pdb” file (from Modeller) in a “.pdbqt” file by using the MGLTools of Autodock [50]. The “.pdbqt” file contained gasteiger charges for every atom present in the original AAC2 “.pdb” file. Similarly, all the ligands “.mol2” files) contained in our chemical library (energetically minimized) were converted in “.pdbqt” files for the virtual screening by using the Autodock scripts [51].

In order to identify the ideal gridbox to be screened with ligands of our library, searching for new putative AAC2 high affinity ligands, firstly we performed ten re-docking simulations [45] by using Autodock 4.2, by varying gridbox size and center, aiming to reproduce the same CATR pose present in the BtAAC1–CATR crystallized complex. According to Sanchez et al. [52] and coordinates reported in the crystallized BtAAC1 for our re-docking simulation we used the β -D-glucoside, namely the (2- α ,8- α ,10- α ,13- α ,15- β)-15-hydroxy-2-[[2-O-(3-methylbutanoyl)-3,4-di-O-sulfo-beta-D-glucopyranosyl]oxy]kaur-16-ene-18,19-dioic acid. For each re-docking simulation the parameter “rmstol” was set to 1.5; the parameter “ga_pop_size” was set to 50, the parameter “ga_num_evals” was set to 2.5×10^5 , the parameter “ga_num_generations” was set to 2.7×10^4 . The number of top individuals to survive to the next generation was set to 5 and a ranked cluster analysis of the 50 ligand poses generated was performed. For details about the significance of the above reported parameter names see Morris et al. [53] or read the tutorials at the following links: <http://autodock.scripps.edu/faqs-help/faq/which-values-of-the-genetic-algorithm-parameters-do-you-normally-use>; http://autodock.scripps.edu/faqs-help/tutorial/using-autodock4-for-virtual-screening/UsingAutoDock4forVirtualScreening_v4.pdf.

The gridbox that better reproduced the pose of the crystallized BtAAC1–CATR complex consists of $40 \times 44 \times 50$ gridpoints in the x - y - z Cartesian space. The distance between each gridpoint of the gridbox was set to 0.281 Å. Obtaining a good re-docked conformation (i.e. a pose of the CATR-ligand within the BtAAC1 binding region very similar to that observed in the crystallized complex) allows establishing residues most likely directly involved in the substrate/inhibitor binding and recognition. The re-docked conformation and the reference CATR inhibitor have been used as a reference system, e.g. to classify all the screened ligands as probable inhibitors or substrates, by using, as discriminant and positive control, the relative binding energy calculated for the best “re-docked” protein–inhibitor conformation.

Table 2

List of the 100 predicted high affinity ligands sorted by energy.

Reference inhibitors and substrates are highlighted in bold characters. "LE_LC" stays for the energy of the lowest energy conformation in the largest cluster identified along autodock runs. K_i represents the inhibition constant calculated by autodock. 2D structures of the assayed ligands are also reported.

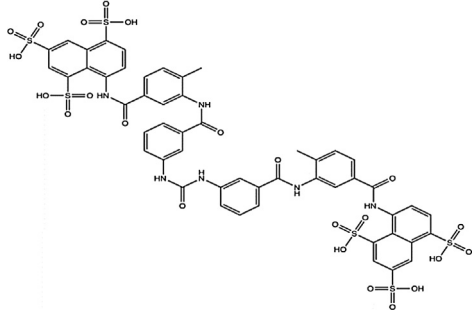
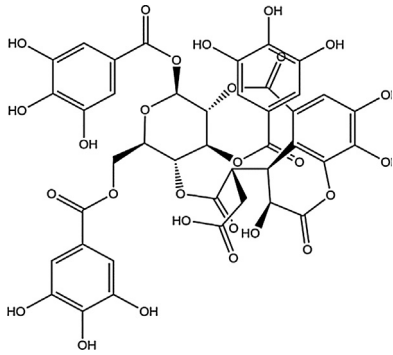
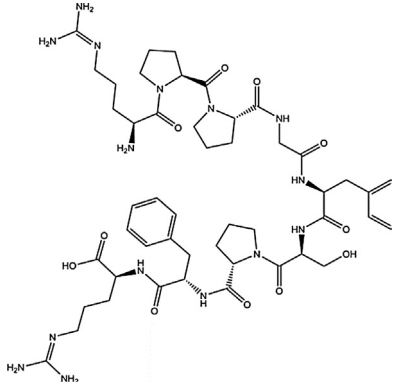
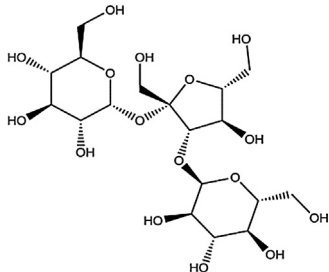
Top list compounds or best binders	Hit	LE_lc	Predicted K_i	2D structures
C07974Suramin	1	-23.8300	3.41 aM	
C08895 CHEBI:4390	2	-21.8800	92.2 aM	
C10233KandelinA-1	3	-20.5800	826.47 aM	
C04900Luteolin	4	-19.0000	11.85 fM	
C06416Precorrin5	5	-19.0800	10.42 fM	
C08984SpinasaponinA	6	-19.0400	3.73 fM	
C10215Chebulinicacid	7	-19.0500	10.91 fM	
C12068GE2270A	8	-19.3900	13.32 fM	
C00306Bradykinin	9	-18.2400	42.32 fM	
C05794I-Urobilin	10	-18.0700	52.27 fM	
ATR Like compounds	Hit	LE_lc	Predicted K_i	2D structures
C08243Melezitose	11	-18.4400	30.47 fM	

Table 2 (Continued)

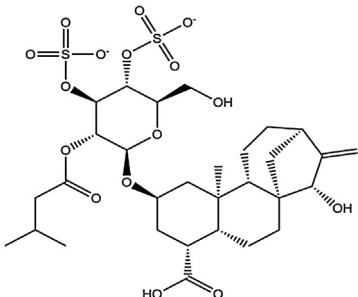
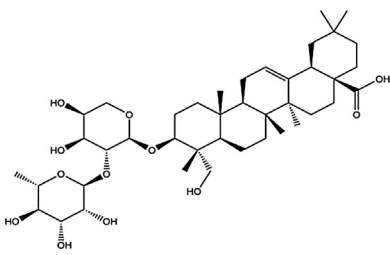
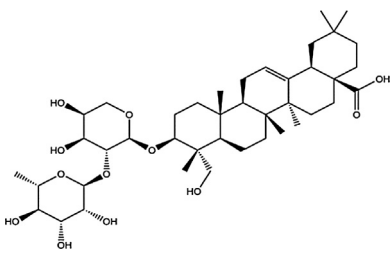
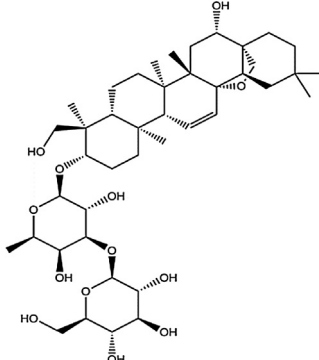
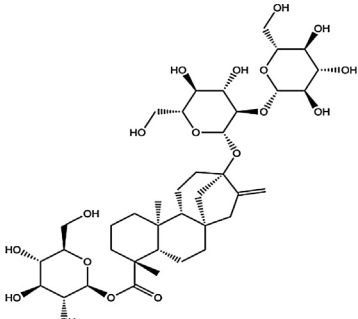
ATR Like compounds	Hit	LE _{1c}	Predicted K _i	2D structures
C08550Iresinin	12	–18.8100	16.16 fM	
C08791CarnosiflosidellI	13	–18.4700	29.13 fM	
C09064Attractyloside	14	–18.3300	36.46 fM	
C09679HelminthosporosideA	15	–18.5200	18.52 fM	
C09972TheasinensinA	16	–18.1900	14.88 fM	
C10100KuwanoneH	17	–18.5800	24.22 fM	
C10318Conocurvone	18	–18.0100	22.38 fM	
C10827Tomatine	19	–18.2100	12.74 fM	
C11712Teprotide	20	–18.7600	17.62 fM	
Stevioside_Like compounds	Hit	LE _{1c}	Predicted K _i	2D structures
C08955beta-Hederin	264	–14.4400	26.14 pM	
C08966PfaffosideA	265	–14.4300	26.57 pM	
CID 167928SaikosaponinA	266	–14.6300	19.02 pM	
C08990YiamolosideB	267	–14.8500	12.98 pM	
C09132Mascaroside	268	–14.4800	24.12 pM	
C09189Stevioside (CID442089)	269	–14.5600	21.28 pM	

Table 2 (Continued)

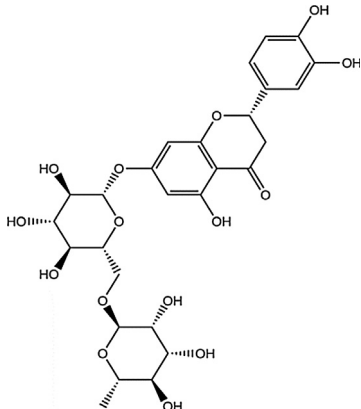
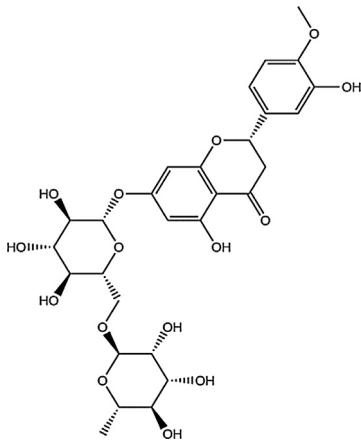
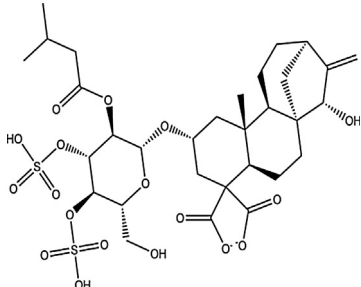
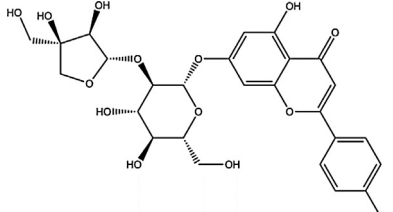
Stevioside_Like compounds	Hit	LE _{1c}	Predicted K _i	2D structures
C09201Tinyatoxin	270	−14.4900	23.83 pM	
C09464Ipecoside	271	−14.6800	17.46 pM	
C09732Eriocitrin	272	−14.6100	19.47 pM	
C09755Hesperidin	273	−14.6900	17.11 pM	
C09761Kolavlanone	274	−14.4400	26.17 pM	
C09834SanggenonC	275	−14.6100	19.55 pM	
Carboxyatractyloside (CATR)_Like compounds	Hit	LE _{1c}	Predicted K _i	2D structures
C15736PatellamideB	320	−14.4400	25.88 pM	
C15737PatellamideD	321	−14.3600	29.8 pM	
C15746Aeruginopeptin228A	322	−14.2400	36.59 pM	
C15763SW163C	323	−14.7400	15.81 pM	
C15764UK63598	324	−14.0800	48.08 pM	
Carboxyatractyloside (SID 134999654)	325	−14.55	21.74 pM	
C15579 Flavanone 7-O-[beta-L-rhamnosyl-(1->2)-beta-D-glucoside]	326	−13.8700	68.28 pM	
C04194 Flavonol 3-O-[beta-L-rhamnosyl-(1->6)-beta-D-glucoside]	327	−13.1300	235.82 pM	
C04858Apigenin 7-O-[beta-D-apiosyl-(1->2)-beta-D-glucoside]	328	−13.5100	124.76 pM	

Table 2 (Continued)

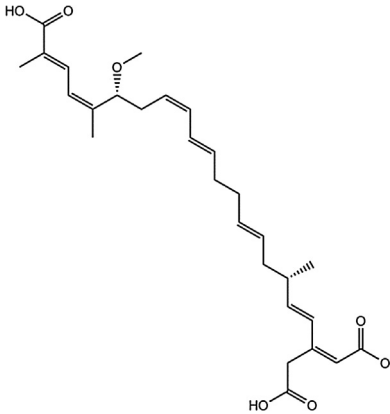
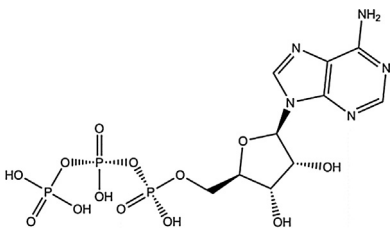
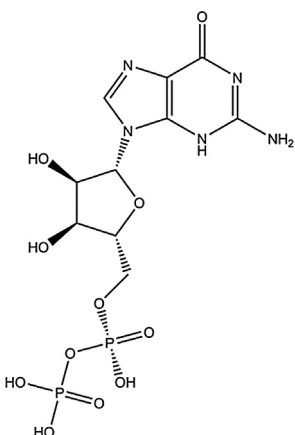
Carboxyatractyloside (CATR)_Like compounds	Hit	LE _{1c}	Predicted K _i	2D structures
C00083Malonyl-CoA	329	-13.0600	267.56 pM	
C00167UDP-glucuronate	330	-13.0100	290.36 pM	
C00323Caffeoyl-CoA	331	-13.0000	294.07 pM	
Bongkreic acid (BKA)_Like compounds	Hit	LE _{1c}	Predicted K _i	2D structures
C15761ConcanamycinA	494	-13.0400	275.89 pM	
C15762OnnamideA	495	-13.7600	81.96 pM	
1'H-5alpha-Cholest-2-eno[3,2-b]indole	499	-12.1800	1.17 nM	
Bongkreic acid CID_6433556	500	-12.8700	365.61 pM	
C00061FMN	501	-12.9100	344.06 pM	
C00075UTP	502	-12.9200	337.79 pM	
C00105UMP	503	-12.0800	1.39 nM	
C00130IMP	504	-12.0400	1.49 nM	
C00185Cellulobiose	505	-12.2700	1.02 nM	
ATP-dATP_Like compounds	Hit	LE _{1c}	Predicted K _i	2D structures
C14325 Dibenz[a,h]anthracene	1270	-10.5500	18.53 nM	
C14951 3-[(2-Chlorobenzylidene)amino]-6H-dibenzo[b,d]pyran-6-one	1271	-10.1600	35.93 nM	
C15466_N-(6-oxo-6H-dibenzo[b,d]pyran-3-yl)maleamic acid	1272	-10.5500	18.51 nM	
C00002ATP	1273	-10.8600	11.02 nM	
C00035GDP	1274	-10.6500	15.51 nM	

Table 2 (Continued)

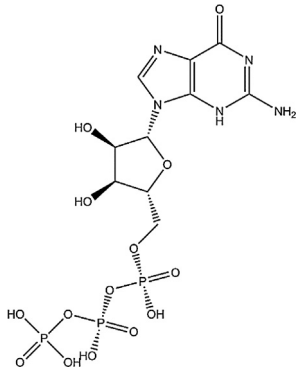
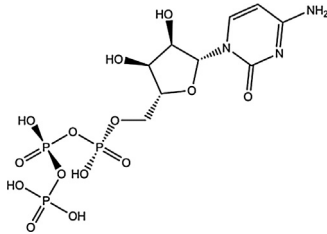
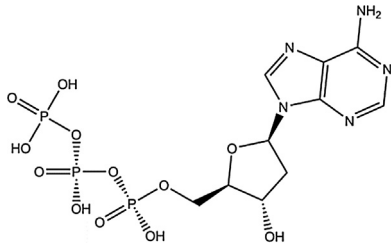
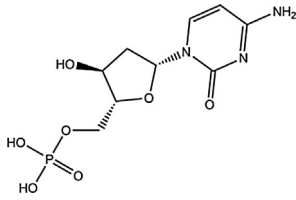
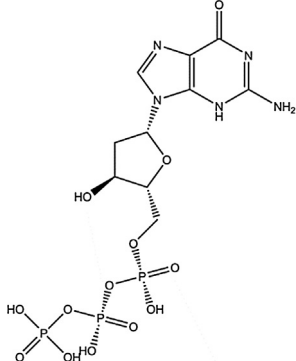
ATP-dATP_Like compounds	Hit	LE _{1c}	Predicted K _i	2D structures
C00044GTP	1275	−10.9600	9.18 nM	
C00063CTP	1276	−10.6700	15.08 nM	
C00068Thiamindiphosphate C00131dATP	1277 1278	−10.2400 −10.1600	31.06 nM 35.97 nM	
C00239dCMP	1279	−10.9800	8.95 nM	
C00255Riboflavin C00286dGTP	1280 1281	−10.800 −10.2600	12.02 nM 30.10 nM	

Table 2 (Continued)

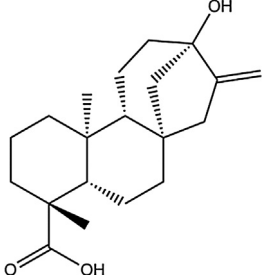
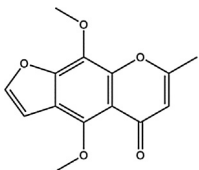
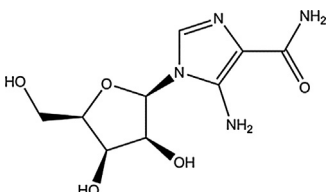
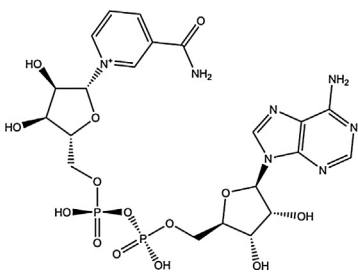
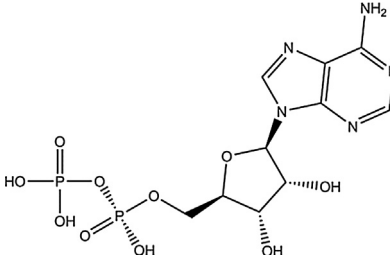
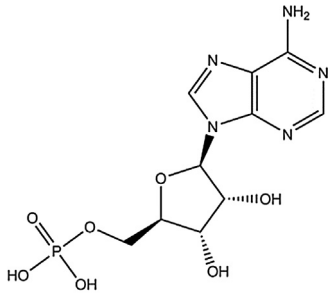
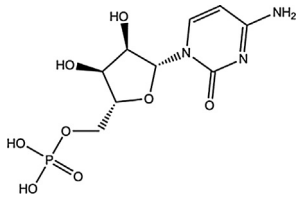
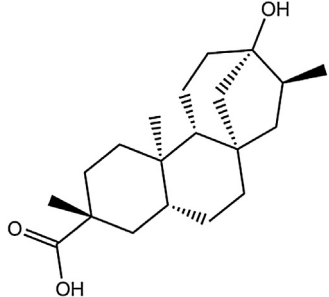
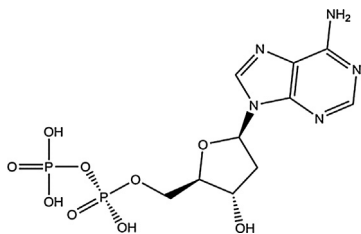
ATP-dATP_Like compounds	Hit	LE _{1c}	Predicted K _i	2D structures
C00294Inosine	1282	−10.4100	23.48 nM	
C00332Acetoacetyl-CoA	1283	−10.1400	36.64 nM	
Steviol_Like compounds	Hit	LE _{1c}	Predicted K _i	2D structures
C15780 5-dehydroepisterol	1968	−10.75	13.18 nM	
Steviol (CID: 452967)	1973	−10.6400	15.75 nM	
CID3828Khellin (deltoside)	1974	−9.5800	97.22 nM	
C15163 17-[(benzylamino)methyl]estra-1,3,5(10)-triene-3,17beta-diol	1975	−9.5200	105.22 nM	
C15177 17-methylandrosta-2,4-dieno[2,3-d]isoxazol-17beta-ol	1976	−9.4600	116.17 nM	
C15050 2,2-dimethyl-3-[4-(acetyloxy)phenyl]-4-ethyl-2H-1-benzopyran-7-ol	1977	−9.3000	151.72 nM	
C04875 (±)-5-[(<i>tert</i> -butylamino)-2'-hydroxypropoxy]-1,2,3,4-tetrahydronaphthol	1978	−9.8000	65.37 nM	
C10482[6]-paradol	1979	−9.1600	193.06 nM	
C04883(±)-5-[(<i>tert</i> -butylamino)-2'-hydroxypropoxy]-3,4-dihydro-1(2H)-naphthol	1980	−9.4600	117.24 nM	
ADP_Like compounds	Hit	LE _{1c}	Predicted K _i	2D structures
AICAR CID46780289	2013	−9.3700	135.86 nM	
C00003NAD+	2015	−9.3000	152.12 nM	
C00006NADP+	2016	−9.1100	208.75 nM	
C00008ADP	2017	−9.4400	119.19 nM	

Table 2 (Continued)

ADP_Like compounds	Hit	LE _{1c}	Predicted K _i	2D structures
C00010CoA	2018	−9.3700	134.94 nM	
C00018Pyridoxalphosphate	2019	−9.1000	214.06 nM	
C00020AMP	2020	−9.7900	66.69 nM	
C00024Acetyl-CoA	2021	−9.9700	48.84 nM	
C00051Glutathione	2022	−9.8100	64.45 nM	
C00055CMP	2023	−9.3200	148.14 nM	
dADP_Like compounds	Hit	LE _{1c}	Predicted K _i	2D structures
Dihydrosteviol	2989	−9.5100	106.16 nM	
FGAR	2990	−9.5900	93.88 nM	
C00166Phenylpyruvate	4190	−9.3000	6.39 μM	
C00206dADP	4192	−9.1100	2.17 μM	

Due to the high percentage of identical residues between BtAAC1 and SLC25A5_AAC2 (more than 89% comparing the full-length sequences; 98% comparing residues of the proposed binding region according to Pierri et al. [44]) we assumed that they share also the same binding region. Thus, we used the same gridbox obtained in the best re-docking simulation within the human AAC2 for screening our ligand library. It was imposed that the gridbox center overlapped with the center of mass of our 3D model resulting to be located approximately between the coordinates of the NZ atom of K23 and the CZ atoms of R80 and R280 of the human AAC2.

In our docking-based virtual screening we chose to use the genetic algorithm [50,54]. For each ligand of our library 30 runs were performed; the parameter “rmstol” was set to 0.5; the parameter “ga_pop_size” was set to 150 and the parameter “ga_pop_evaluations” was set to 1.7×10^6 . The simulation was performed on a dedicated server (motherboard Extreme/NSE Striker II mounting an Intel Core™ 2 Quad Processor (till 2.4 GHz of frequency) and 8GB of ram 1333 MHz Front Side Bus), which needed 2 months for completing the screening of the entire library.

At the end of the simulation we built a list sorted by energy of the lowest energy docking for each ligand for a total of 6492 successfully screened ligands (the complete list is available upon request). Thus, we searched for ligands bound to AAC2 with the lowest energy (best binders) at the top of the list. Furthermore, we searched for our reference inhibitors and substrates and we selected several ligands with a calculated “binding energy” comparable to that shown by known AAC2 inhibitors (ATR, CATR, BKA, STE) and substrates (ATP and/or ADP).

2.8. Other experimental procedures

Protein was analyzed by SDS-PAGE and stained with Coomassie Blue dye. N-terminal sequencing was carried out as described previously [55]. The amount of pure AAC2 was estimated by laser densitometry of stained samples, using carbonic anhydrase as protein standard [56]. The amount of protein incorporated into liposomes was measured as described previously [55] and was about 20% of the protein added to the reconstitution mixture. For investigating the selectivity of AAC2 inhibitors, transport assays in presence and absence of the selected inhibitors were also performed on three other MCs, namely the human ATP-Mg/P_i carrier (APC1, RefSeq accession number: NP_037518.3), the human aspartate/glutamate carrier (AGC1, RefSeq accession number: NP_003696.2) and the human ornithine carrier (ORC1, RefSeq accession number: NP_000378.1). The overproduction of APC1, AGC1 and ORC1 as inclusion bodies in the cytosol of *E. coli* was accomplished as described previously [57–59]. The functional reconstitution and the transport activity of APC1, AGC1 and ORC1 were carried out according to protocols described previously [57–59].

3. Results

3.1. Bacterial expression of AAC2

The AAC2 open reading frame was expressed in *E. coli* BL21(DE3) cells (Fig. 1, lane 4) and the gene product, accumulated as inclusion bodies, was purified by ultracentrifugation and washing. The apparent molecular mass of the purified protein was 31 kDa, in good agreement with its theoretical molecular mass (calculated value with initiator methionine, 32.7 kDa) (Fig. 1, lane 5). The yield of the purified protein was approximately 40 mg per liter of culture. The protein was not detected neither in bacteria harvested immediately before the induction of the expression vectors (Fig. 1,

lanes 1 and 2) nor in cells harvested after induction lacking the coding sequence in the expression vector (Fig. 1, lane 3).

3.2. Functional characterization of the human recombinant AAC2 in proteoliposomes

The transport of ATP and ADP of the human recombinant AAC2 was tested in homo-exchange experiments (*i.e.* with the same substrate internally and externally). Using internal and external substrate concentrations of 10 and 0.1 mM, respectively, the reconstituted protein catalyzed active [³H]ATP/ATP and [¹⁴C]ADP/ADP exchanges that were inhibited completely by a mixture of pyridoxal 5'-phosphate and bathophenanthroline (data not shown). Despite of the long incubation period (*i.e.* 30 min) very little homo-exchange activity was instead observed for AMP, GTP, UTP, CTP (data not shown). Importantly, no [³H]ATP/ATP and [¹⁴C]ADP/ADP exchange activities were detected when AAC2 has been boiled before incorporation into liposomes or when proteoliposomes were reconstituted with sarkosyl-solubilized material from bacterial cells either lacking the expression vector for AAC2 or harvested immediately before induction of expression (data not shown). Notably, the above-mentioned homoexchanges were null using liposomes without incorporated protein (data not shown). All the provided controls demonstrate the integrity of our proteoliposomes.

The substrate specificity of AAC2 was investigated by measuring the initial rate of [³H]ATP uptake into proteoliposomes that had been preloaded with various potential substrates (Fig. 2). The highest activities of ATP uptake into proteoliposomes were found with internal ATP and ADP. To a lesser extent [³H]ATP also exchanged with internal dATP and dADP.

The uptake of [³H]ATP was instead very low in the presence of the following internal substrates: AMP, GMP, CTP, CDP, UTP, and was negligible in the presence of internal, dAMP, GTP, GDP, CMP, UDP, UMP, TTP, TDP, TMP, NADH, FAD, phosphate (Pi), or in uniport

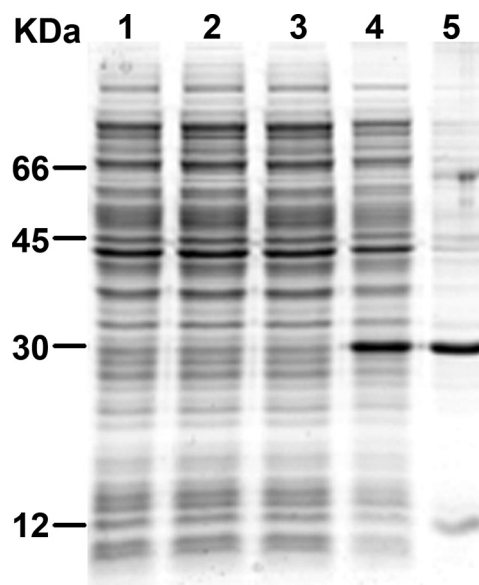


Fig. 1. Bacterial overexpression in *E. coli* and purification of AAC2. Proteins were separated by SDS-PAGE and stained with Coomassie Blue dye. Markers in the left-hand column were bovine serum albumin, ovalbumin, bovine carbonic anhydrase and cytochrome c; lanes 1–4, *E. coli* BL21 (DE3) containing the expression vector without (lanes 1 and 3) and with (lanes 2 and 4) the coding sequence of AAC2. Samples were taken immediately before (lanes 1 and 2) and 4 h after induction (lanes 3 and 4) from bacterial extract. The same number of bacteria was analysed in each sample. Lane 5, purified AAC2 (about 4 µg).

experiments (*i.e.* in the absence of internal substrate using only NaCl, Fig. 2). Our results about substrate specificity are consistent with previously reported data about other human AACs [12,60,61] or AACs from other species [62] indicating that AACs translocate specifically ADP and ATP at variance with other human nucleotide mitochondrial carriers also involved in the translocation of dinucleotides and cofactors [37–39,59].

The inhibitory effect of nucleotides on the [³H]ATP/ATP exchange reaction catalyzed by reconstituted AAC2 was also examined. The uptake of radio-labeled ATP was measured in the presence of a 20-fold excess of a non-labeled compound (Fig. 3). High transport inhibition was observed with external added (non-labeled) ATP and ADP. The [³H]ATP uptake was inhibited about 75% and 65% in the presence of dATP and dADP, respectively. Furthermore, about 15% of inhibition in the transport rate was observed with external AMP and dAMP.

The guanosine tri- and di-phosphate nucleotides reduced the rate to about 45%, but the corresponding monophosphate nucleotide showed very low effect. Also, the pyrimidine nucleotides reduced the [³H]ATP uptake with the following order of efficiency XTP > XDP > XMP (“X” staying for U, T, C pyrimidines). These results confirm that nucleotides should host at least two phosphate groups for being recognized by AAC2 and for inhibiting the [³H]ATP uptake (Fig. 3).

3.3. Kinetic characteristics of the human recombinant AAC2

The time-courses of 0.1 mM [³H]ATP or [¹⁴C]ADP uptake into liposomes reconstituted with AAC2 were compared either as uniport (in the absence of internal substrate) or as exchange (in the presence of 10 mM ATP or ADP, respectively) (Fig. 4).

Both [³H]ATP/ATP and [¹⁴C]ADP/ADP exchanges followed a first-order kinetics with rate constants 0.36 and 0.37 min⁻¹ and initial rates 1.41 and 1.48 mmol/(min × g protein), respectively, with isotopic equilibrium being approached exponentially, while the uniport uptake of ATP or ADP was negligible (Fig. 4).

The Michaelis–Menten (half-saturation) constant (K_m) of the human reconstituted AAC2 were determined by measuring the

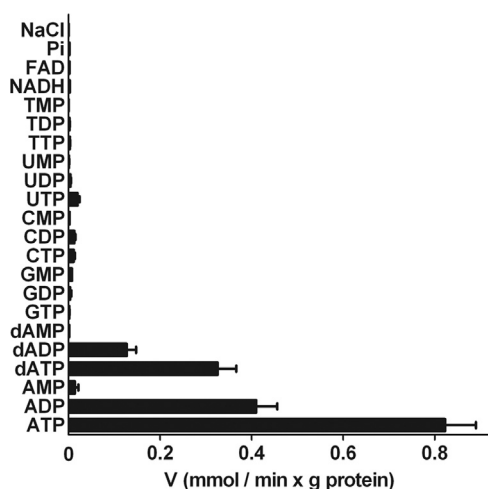


Fig. 2. Dependence on internal substrate of the transport properties of proteoliposomes reconstituted with the human recombinant AAC2.

Proteoliposomes were preloaded internally with various substrates (each substrate was preloaded at the final concentration of 10 mM). Transport was started by adding 0.012 mM [³H]ATP to liposomes reconstituted with AAC2 and stopped after 30 s. Reported data are the means ± S.D. of at least three independent experiments. Abbreviations: Pi: phosphate dATP: deoxyATP; dADP: deoxyADP; dAMP: deoxyAMP.

initial substrate transport rate by varying the external [³H]ATP or [¹⁴C]ADP concentrations in the presence of a fixed internal saturating concentration (10 mM) of ATP or ADP. The K_m for ATP and ADP were 11.6 ± 0.9 μM and 32.1 ± 4.0 μM, respectively, and the V_{max} values were 1.91 ± 0.22 mmol/(min × g protein) and 1.93 ± 0.28 mmol/(min × g protein).

3.4. Effect of highly selective AAC inhibitors on the human recombinant AAC2

We have investigated the effect of the known/proposed highly selective AAC inhibitors, *i.e.* CATR, BKA, STE and STD [25,30] on transport catalyzed by the human recombinant AAC2.

Fig. 5a shows the residual activity of the [³H]ATP/ATP exchange in proteoliposomes reconstituted with AAC2 at pH 7.0 in presence of different external concentrations of CATR, BKA, and STE. In presence of CATR, the residual transport activity at pH 7.0 is about 50% at CATR 0.01 μM and 10% at CATR 0.1 μM. A 70% of residual activity, is observed at CATR 0.005 μM and a negligible inhibition is observed at CATR 0.001 μM.

A residual transport activity of about 50% was observed in presence of BKA 2.5 μM and 10% at BKA 10 μM. In presence of BKA 0.1 μM the inhibition was very low (residual transport activity of about 80%). Furthermore, we observed about the 50% of AAC2 inhibition in presence of STE 50 μM and about 70% in presence of STE 100 μM (Fig. 5a). Finally, STD did not show any inhibition of the [³H]ATP/ATP exchange catalyzed by the recombinant AAC2 (data not shown).

In mitochondria of rat heart, it was demonstrated that the inhibition of BKA is strictly dependent on changes in temperature and pH. In particular, the BKA inhibition is markedly increased at pH lower than 7.0 [63]. In light of these observations, the BKA inhibition of [³H]ATP uptake was also tested at pH 6.2. Notably, we observed that at pH 6.2 the transport activity of the recombinant AAC2 is the same as that at pH 7.0, but the inhibition of transport is about 80% in the presence of 2.5 μM BKA and about 50% in the presence of 0.5 μM of BKA (data not shown). These results confirm the pH dependence of the BKA inhibition of ATP transport catalyzed by AAC2. The same results were obtained monitoring

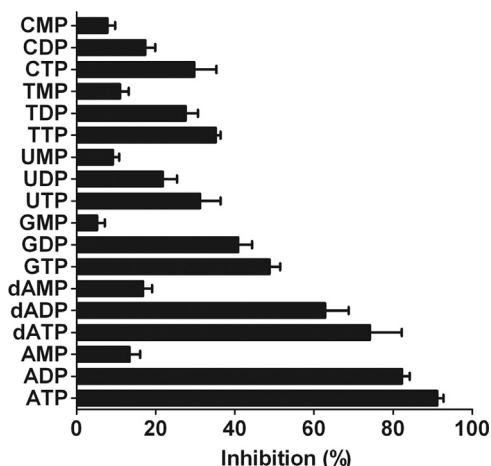


Fig. 3. Inhibition of the rate of [³H]ATP uptake by external substrates.

Liposomes reconstituted with recombinant AAC2 were preloaded internally with 10 mM ATP. Transport was started by adding 0.012 mM [³H]ATP and stopped after 30 s. External substrates (concentration, 0.24 mM) were added together with [³H]ATP. The indicated values are expressed as a percentage of the [³H]ATP/ATP exchange activity and are the means of at least three independent experiments. The mean value of [³H]ATP/ATP exchange activity is 0.81 ± 0.09 mmol/(min × g protein).

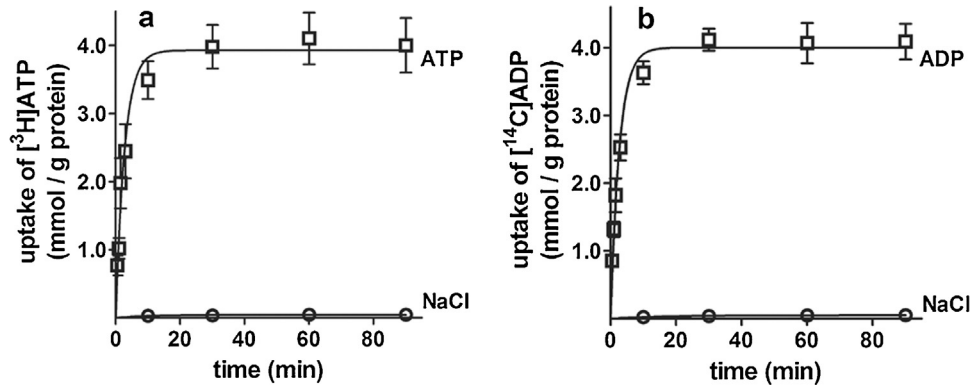


Fig. 4. Kinetics of [^3H]ATP and [^{14}C]ADP transport in proteoliposomes reconstituted with AAC2.

Panel a, uptake of [^3H]ATP and panel b, uptake of [^{14}C]ADP. 0.1 mM [^3H]ATP in “a” or 0.1 mM [^{14}C]ADP in “b” was added to proteoliposomes containing 10 mM ATP in “a” or ADP in “b” (exchange, \square) or 10 mM NaCl and no substrate (uniport, \circ). Indicated values are the means of at least three independent experiments.

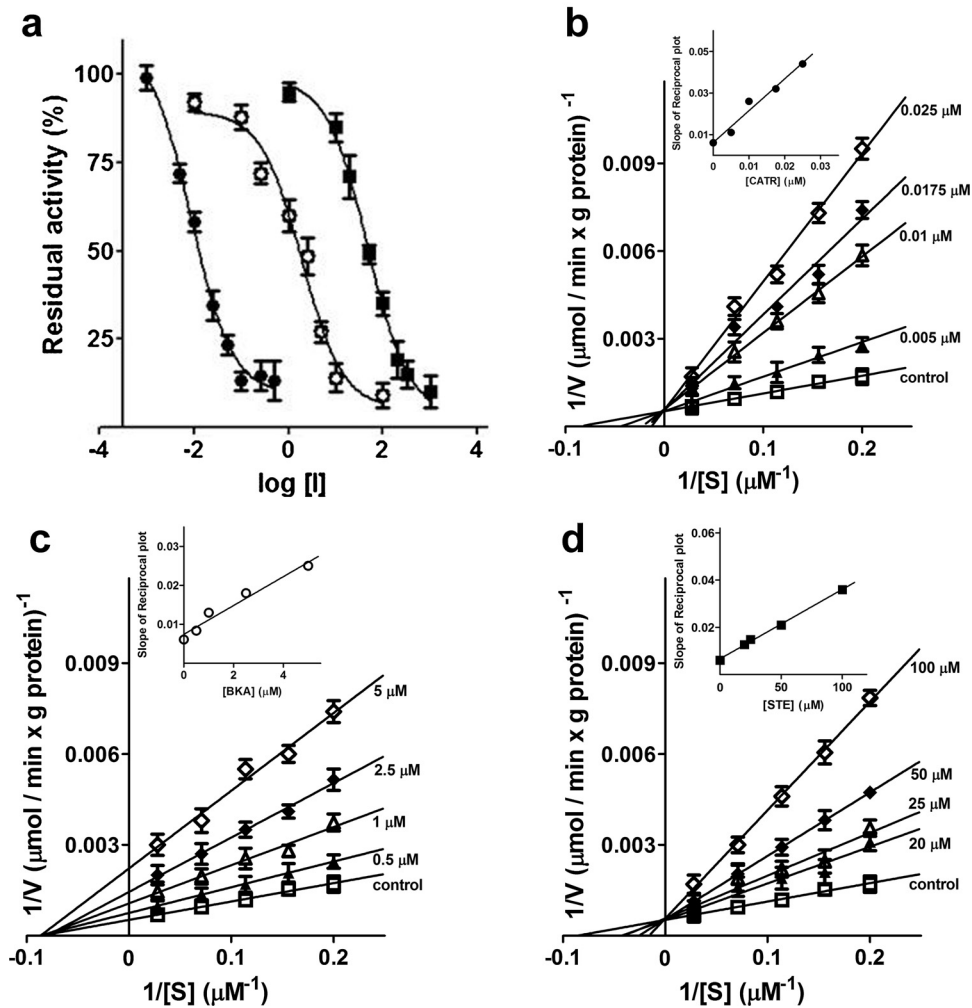


Fig. 5. Inhibition of the rate of [^3H]ATP uptake in presence of CATR, BKA and STE.

AAC2-reconstituted liposomes were preloaded internally with 10 mM ATP. Panel a. Determination of CATR, BKA and STE IC_{50} : transport was initiated by adding 0.012 mM [^3H]ATP together with increasing external concentration of CATR (\bullet ; 0.001, 0.005, 0.01, 0.025, 0.05, 0.1, 0.25 and 0.5 μM), BKA (\blacksquare ; 0.01, 0.1, 0.25, 1, 2.5, 5, 10, 100 μM) and STE (\blacksquare ; 0.001, 0.01, 0.02, 0.05, 0.1, 0.2, 0.3, 1 mM). The reaction time was 30 s. The residual transport activity (%) in presence of each inhibitor results from the average of at least three independent experiments. The mean value of [^3H]ATP/ATP exchange activity is 0.81 ± 0.09 mmol/(min \times g protein). Panels b–d: Lineweaver–Burk plots reporting the uptake of [^3H]ATP at the indicated concentrations into preloaded proteoliposomes in the absence (\square) or in the presence of 0.005 μM (\blacktriangle), 0.01 μM (\triangle), 0.0175 μM (\blacklozenge), and 0.025 μM (\diamond) of CATR (panel b); 0.5 μM (\blacktriangle), 1 μM (\triangle), 2.5 μM (\blacklozenge), and 5 μM (\diamond) of BKA (panel c) 20 μM (\blacktriangle), 25 μM (\triangle), 50 μM (\blacklozenge), and 100 μM (\diamond) of STE (panel d) externally added. The inserts represent the secondary plots of the slopes of Lineweaver–Burk plots obtained at the indicated concentrations of CATR (\bullet panel b), BKA (\circ panel c) and STE (\blacksquare panel d) used for determining the inhibition constants K_i .

the [^{14}C]ADP/ADP exchange in proteoliposomes reconstituted with AAC2 (data not shown).

3.5. Kinetic analysis of recombinant AAC2 inhibition

We further characterized the inhibition mechanism of these inhibitors by using double-reciprocal plots obtained by analysing the rate of the uptake of various external [^3H]ATP concentrations into proteoliposomes reconstituted with the human AAC2 (at constant internal ATP concentration of 10 mM), in presence and absence of different concentrations of CATR, BKA and STE. Fig. 5 panels b–d report Lineweaver–Burk plots of [^3H]ATP uptake in presence of increasing concentrations of CATR, BKA and STE, respectively.

Fig. 5b reveals that CATR is a competitive inhibitor as increased the apparent K_m without changing the V_{\max} of the [^3H]ATP/ATP exchange. Furthermore, the K_i value for CATR, estimated by secondary plot using four different inhibitor concentrations (0.005, 0.01, 0.0175 and 0.025 μM), was equal to 0.004 μM (see the insert of Fig. 5b), as also obtained by the rate Eq. (4).

Similarly a primary Lineweaver–Burk plot revealed that the BKA is a non competitive inhibitor. The K_i of BKA for AAC2 obtained from a secondary plot by using four concentrations of BKA (0.5, 1, 2.5 and 5 μM) was 2.0 μM at pH 7.0, in agreement with K_i obtained according to the reported rate Eq. (5).

In presence of STE we observed a competitive inhibition (Fig. 5c). Also for building the secondary plot about STE inhibition we used four STE concentrations (20, 25, 50 and 100 μM). We observed a K_i of 22.5 μM , thus STE is less specific than CATR and BKA for AAC2. The obtained K_i is similar to the K_i obtained according to the reported rate Eq. (4).

3.6. Re-docking and virtual screening

The re-docking simulation allowed us to define a specific gridbox (see Section 2.7) for the BtAAC1 that reproduced the crystallized protein–inhibitor complex with high fidelity. The root mean square deviation (RMSD) between the coordinates of the ligand in the crystallized complex and the best “re-docked” pose coordinates, obtained by using Autodock, was equal to 1.1 Å (data not shown). Given the high percentage of identical amino acids that BtAAC1 shares with the human AAC2, we decided to use the same gridbox for performing a docking-based virtual screening of our chemical library on the human AAC2 3D comparative model. The list sorted by energy of the 6492 successfully screened ligands is available upon request. The first 10 ligands of the list are the best binders (Table 2). Furthermore, we searched along the list of the screened ligands for our reference inhibitors and substrates and we selected 10–12 ligands/candidates “energetically close” to reference inhibitors/substrates for a total of 100 ligands/candidates (Table 2). All the 100 ligands were structurally related to the reference inhibitors/substrates and showed a calculated “binding energy” comparable to that shown by known AAC2 reference inhibitors (ATR, CATR, BKA, STE, see Table 2) and substrates (ATP, ADP, dATP, dADP, see Table 2). From the above selected 100 ligands we chose 13 commercially available molecules for testing them in transport assays on the AAC2 recombinant protein.

3.7. The effect of the predicted high affinity ligands on AAC2 activity

The effect of the 13 selected compounds on the activity of the human AAC2 was examined by monitoring the [^3H]ATP/ATP homoechange in the presence of 120 μM (about 10 fold the K_m for ATP) of the proposed inhibitors. The [^3H]ATP/ATP exchange reaction was inhibited strongly by chebulinic acid, suramin and partially by saikosaponin (analogue of STE/STD) and melezitose

(analogue of ATR) (Fig. 6). In contrast, the AAC2-mediated [^3H]ATP/ATP exchange was inhibited very poorly by all the other molecules tested (Fig. 6). The inhibition of the [^3H]ATP/ATP exchange in proteoliposomes reconstituted with AAC2 was further investigated in the presence of increasing concentrations of the most active inhibitors (chebulinic acid, suramin and saikosaponin, Fig. 7a) added externally to the proteoliposomes.

As shown in Fig. 7a, the residual AAC2 transport activity (%) was graphed against the corresponding \log_{10} inhibitor concentration and a residual activity of about 50% of the [^3H]ATP/ATP exchange was obtained with about 0.8 μM , 4 μM , and 240 μM of suramin, chebulinic acid, and saikosaponin, respectively (Fig. 7a). Since saikosaponin did not affect severely AAC2 activity, we focused our attention on the other two stronger AAC2 inhibitors, chebulinic acid and suramin, by estimating their K_i for AAC2.

External addition of increasing concentrations of chebulinic acid or suramin, in presence of radiolabeled ATP, to proteoliposomes reconstituted with the recombinant AAC2, allowed to build Lineweaver–Burk plots showing that both compounds were competitive inhibitors of AAC2, as they increased the apparent K_m without changing the V_{\max} of the [^3H]ATP/ATP exchange (Fig. 7 panels b and c). The K_i of suramin and chebulinic acid for AAC2 were obtained by building a secondary plot for each inhibitor (inserts within Fig. 7b and c). Four suramin (0.1, 0.2, 0.4, 1 μM) and chebulinic acid (1.2, 4, 8, 20 μM) concentrations were employed for building the two corresponding secondary plots. The obtained K_i were 0.3 μM and 2.1 μM , respectively.

3.8. Effect of chebulinic acid and suramin on different mitochondrial carriers

To verify if chebulinic acid and suramin are selective inhibitors of AAC2, we analysed the effect of these compounds also on the activity of other human mitochondrial carriers. With this aim, transport assays were performed on APC1, ORC1 and AGC1 in presence and absence of the newly proposed AAC2 inhibitors (chebulinic acid and suramin). These mitochondrial carriers were

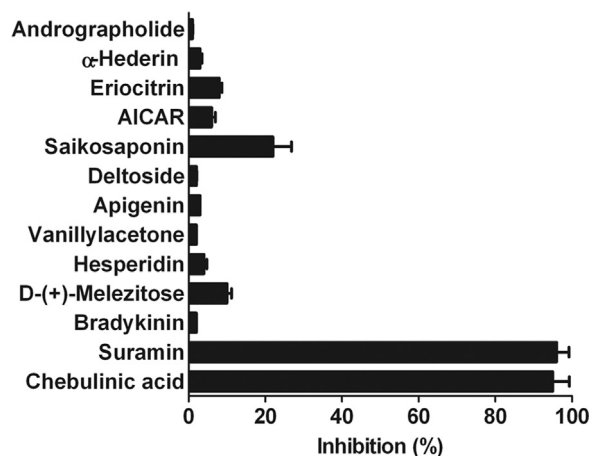


Fig. 6. Effect of the new predicted inhibitors on the [^3H]ATP/ATP exchange mediated by the human recombinant AAC2.

The putative inhibitors (0.120 mM each) were tested on [^3H]ATP/ATP exchange in proteoliposomes reconstituted with recombinant AAC2 preloaded with 10 mM ATP. The transport was started by adding 0.012 mM [^3H]ATP and was stopped after 30 s. The inhibition values are calculated as a percentage of the [^3H]ATP/ATP exchange activity and are the means of at least three independent experiments. The mean value of [^3H]ATP/ATP exchange activity is 0.84 ± 0.12 mmol/(min \times g protein). Abbreviation: AICAR: 5-aminoimidazole-4-carboxamide ribonucleotide. Deltoside is commonly used as a synonym for many compounds, the ligand within our library is commercially known as khellin (sigma code: 60730). In place of the not commercially available Apigenin 7-O-[beta-D-apiosyl-(1->2)-beta-D-glucoside] here we used its precursor Apigenin 7-glucoside (sigma code: 44692).

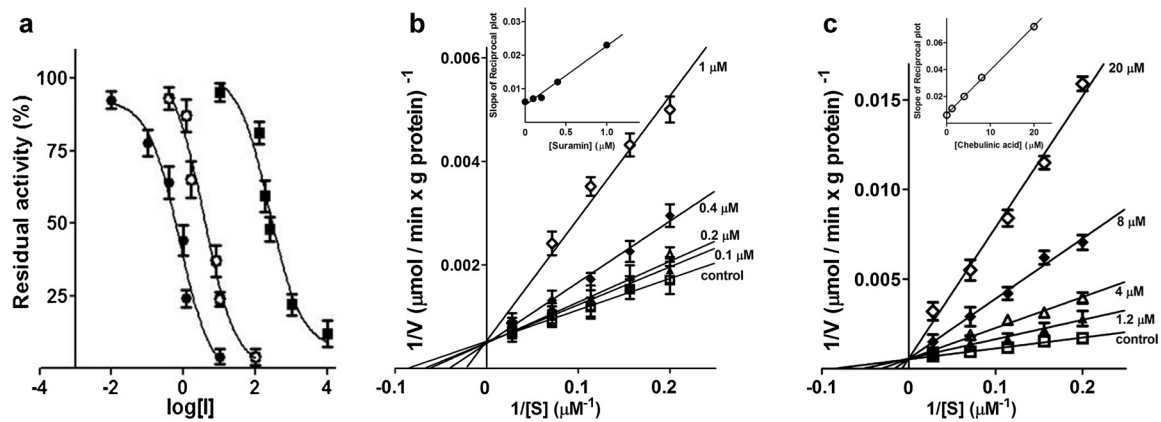


Fig. 7. Inhibition of the rate of $[^3\text{H}]\text{ATP}$ uptake in presence of the newly proposed inhibitors, suramin and chebulinic acid. Proteoliposomes were preloaded internally with 10 mM ATP. Panel a. Determination of IC_{50} : inhibition of $[^3\text{H}]\text{ATP}/\text{ATP}$ exchange by increasing concentrations of chebulinic acid (\circ ; 0.4, 1.2, 1.6, 8, 10, and 100 μM), suramin (\bullet ; 0.01, 0.1, 0.4, 1, 1.2, and 10 μM) and saikosaponin (\blacksquare ; 0.01, 0.125, 0.180, 0.250, 1, 10 mM). Transport was started by adding 0.012 mM $[^3\text{H}]\text{ATP}$ and stopped after 30 s. Inhibitors were added together with the radiolabeled substrate. The residual transport activity (%) in presence of each inhibitor results from the average of at least three independent experiments. The mean value of $[^3\text{H}]\text{ATP}/\text{ATP}$ exchange activity is 0.78 ± 0.07 mmol/(min \times g protein). Panels b and c: Lineweaver–Burk plots reporting the uptake of $[^3\text{H}]\text{ATP}$, at the indicated concentrations, into preloaded proteoliposomes in the absence (\square) or in the presence of 0.1 μM (\blacktriangle), 0.2 μM (\triangle), 0.4 μM (\blacklozenge), and 1 μM (\diamond) of suramin (panel b), 1.2 μM (\blacktriangle), 4 μM (\triangle), 8 μM (\blacklozenge), and 20 μM (\diamond) of chebulinic acid (panel c) externally added. The inserts represent the secondary plots of the slopes of Lineweaver–Burk plots obtained at the indicated concentrations of suramin (\bullet panel b), and chebulinic acid (\circ panel c) used for determining the inhibition constant K_i .

chosen for their different substrate specificity (APC1 translocates nucleotides and phosphate; ORC1 translocates basic amino acids; AGC1 translocates acidic amino acids [57–59]).

The inhibitors were tested on the exchanges $[^{14}\text{C}]\text{ADP}/\text{P}_i$ for APC1, $[^{14}\text{C}]\text{aspartate}/\text{aspartate}$ for AGC1 and $[^3\text{H}]\text{ornithine}/\text{ornithine}$ for ORC1 using the concentration of radiolabeled substrates corresponding to the APC1, AGC1 and ORC1 K_m values, according to our protocols [57–59].

For evaluating the selectivity of chebulinic acid and suramin, we performed the above cited transport assays in presence of 10 μM of each inhibitor. We chose the concentration of 10 μM because it represents an inhibitor concentration threshold (for our best inhibitors CATR, BKA, chebulinic acid and suramin) that completely inhibits AAC2. In these experiments the homoexchange of $[^3\text{H}]\text{ATP}/\text{ATP}$ mediated by the human AAC2 was used as a control.

In Fig. 8 it is shown that 10 μM of CATR, BKA, chebulinic acid and suramin inhibit the AAC2 transport activity of the 80–95%.

Conversely, APC1 is inhibited of $9.0 \pm 0.9\%$ in presence of BKA, $15.3 \pm 3.2\%$ in presence of CATR, $21.2 \pm 3.3\%$ in presence of chebulinic acid and $27.8 \pm 5.2\%$ in presence of suramin, confirming the low affinity of the investigated ligands for APC1 (Fig. 8). ORC1 inhibition in presence of the four proposed inhibitors is lower than 5% (Fig. 8). CATR and BKA inhibit very poorly AGC1, but the $[^{14}\text{C}]\text{aspartate}/\text{aspartate}$ homoexchange (AGC1 mediated) is inhibited of about $40.8 \pm 5.3\%$ and $45.3 \pm 4.2\%$ in presence of chebulinic acid and suramin, respectively (Fig. 8).

4. Discussion

Mitochondrial apoptosis is triggered by the opening of the mitochondrial PTP. Notably, AACs play a crucial role in regulating PTP opening due to their involvement in the ATP transfer to the cytosol from mitochondria [9,64–66].

Four genes encoding AACs were identified in *H. sapiens*. Among the four paralogs, AAC2 is involved in the maintenance of mitochondrial membrane potential and in preventing apoptosis [7–9,21]. Notably, AAC2 was found upregulated in several hormone-dependent cancers [14] and is specifically involved in

glycolytic metabolism of cancer cells [21]. Thus, AAC2 could represent a new molecular target to be inhibited for treating cancer. The concept of AAC2 as a therapeutic target for anti-cancer therapy has also been validated in a preclinical colon cancer xenograft mouse model [19,67–70] in which it was shown that the suppression of AAC2 exerts anticancer effects [19]. Therefore, identifying new selective AAC inhibitors could allow the development of new therapeutic strategies for cancer treatment. In order to kinetically characterize the human recombinant AAC2 we

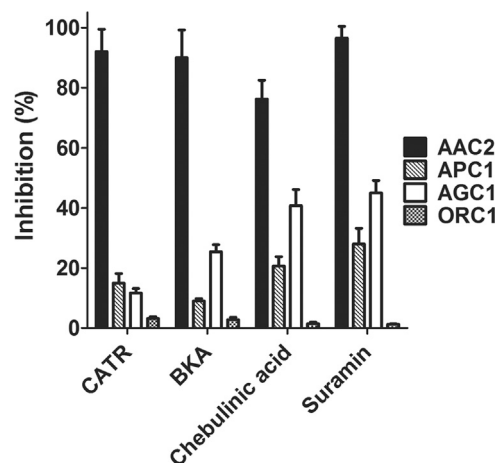


Fig. 8. Inhibition of the exchange activity of recombinant AAC2, APC1, AGC1 and ORC1 proteins.

Each recombinant protein was reconstituted in proteoliposomes preloaded with 10 mM of internal ATP for AAC2, P_i for APC1, aspartate for AGC1 and ornithine for ORC1. 10 μM of CATR, BKA, chebulinic acid or suramin were added together with the external radiolabeled specific substrate at the corresponding K_m concentration: 0.012 mM of $[^3\text{H}]\text{ATP}$ for AAC2, 0.05 mM $[^{14}\text{C}]\text{aspartate}$ for AGC1, 0.3 mM of $[^{14}\text{C}]\text{ADP}$ for APC1 and 0.22 mM $[^3\text{H}]\text{ornithine}$ for ORC1. The reaction was stopped at the time corresponding to the initial linear range of substrate uptake for each carrier. The inhibition values (%) are means of at least three independent experiments. Exchange activity control values are for APC1 $[^{14}\text{C}]\text{ADP}/\text{P}_i$ 0.185 ± 0.019 mmol/(min \times g protein); for AGC1 $[^{14}\text{C}]\text{aspartate}/\text{aspartate}$ 0.03 ± 0.002 mmol/(min \times g protein); and for ORC1 $[^3\text{H}]\text{ornithine}/\text{ornithine}$ 1.65 ± 0.13 mmol/(min \times g protein).

estimated kinetics parameters of AAC2 substrates, *i.e.* ADP and ATP, and inhibitors, *i.e.* CATR, BKA, STE, STD, by transport assays on AAC2 proteoliposomes.

4.1. Kinetic parameters of the translocated substrates and known inhibitors

The calculated K_m of ATP and ADP for AAC2 are consistent with the range of K_m values measured in rat liver mitochondria [60,71] and in *E. coli* membranes [61]. Few observed discrepancies with previous works can be ascribed to the different systems (intact mitochondria or *E. coli* membranes) employed for AAC characterization. It should be stressed that the K_m of ATP and ADP (as well as K_i of the investigated inhibitors) estimated in our transport assays for AAC2 should strictly depend on AAC2 activity, given that no [^3H]ATP/ATP and [^{14}C]ADP/ADP exchange activities were detected when AAC2 has been boiled before incorporation into liposomes or when proteoliposomes were reconstituted with sarkosyl-solubilized material from bacterial cells either lacking the expression vector for AAC2 or harvested immediately before induction of expression.

Notably, the K_m values of ATP and ADP for AAC4 [12] were higher than K_m of ATP and ADP we observed for AAC2, although considering that Dolce et al. used a protocol similar to ours [12]. Nevertheless, AAC4 is the more dissimilar paralog among the four human AACs. Indeed AAC4 has a long N-terminus portion and shares only the 65% of identical residues with AAC1 and AAC2.

Thus, the reported higher K_m of ATP and ADP for AAC4 could be ascribed to the different overall AAC4 amino acid composition.

Concerning inhibitors, it is the first time that K_i of CATR and BKA for AAC2 are estimated on the human recombinant AAC2 through transport assays on proteoliposomes. At pH 7.0, we observed that CATR was a competitive powerful inhibitor ($K_i=4.0\text{ nM}$) also according to what observed from Klingenberg on mitochondria [31], BKA was a non competitive inhibitor ($K_i=2.0\text{ }\mu\text{M}$) also according to what observed from Vignais on mitochondria [63], STE was a competitive relatively weak inhibitor ($K_i=22.5\text{ }\mu\text{M}$), whereas STD is not able to inhibit AAC2 at all. From this first determination, we can state that CATR, BKA and STE are good AAC inhibitors, whereas STD is not. Notably, it was recently proposed that STD has antitumor activity [72] but we retain that the effects observed by Paul et al., although depending on AAC inhibition, should be due to the STE obtained from STD hydrolysis [73]. It was also proposed that STD inhibits (weakly) ATP synthesis through assays on intact mitochondria [30]. Nevertheless, also in that case we retain that the observed effects should be ascribed to the STD hydrolysis product, namely STE. Other differences observed in CATR or STE inhibition mechanism from Vignais et co. could also be ascribed to the synergic action of other bioactive compounds present in Atractylis and Stevia extracts and to the assays performed by monitoring ATP synthesis on mitochondria [30,74].

Concerning BKA it was proposed that it can inhibit AAC from the matrix side [25]. We can observe that BKA inhibits AAC2 in a non competitive way, thus we can speculate that it can bind a region

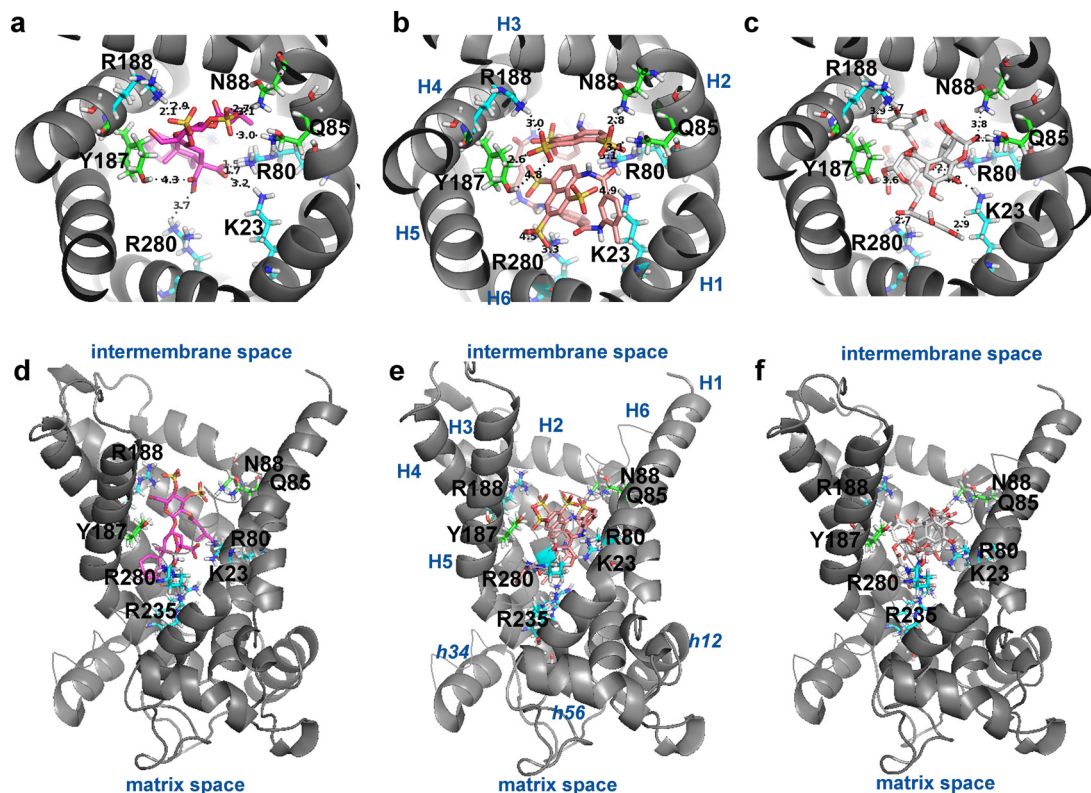


Fig. 9. Top and side views of the human AAC2 in presence of CATR (panels a and d), suramin (panels b and e) and chebulinic acid (panels c and f). In the three top views AAC2 is reported in grey cartoon representation. In the three side views AAC2 transmembrane helices H1–H5 and little helices h12, h34, h56 are reported in grey cartoon representation, whereas H6 is reported in grey ribbon representation for allowing the carrier cavity inspection. For facilitating protein–ligand complex inspection, in the central panels of the figure transmembrane helices and little helices are also indicated by blue labels. Hydrophilic residues within 4 Å from the shown inhibitors are reported in green sticks representation and labeled. Basic residues within 4 Å from the shown inhibitors are reported in cyan sticks representation and labeled. CATR (2- α ,8- α ,10- α ,13- α ,15- β)-15-hydroxy-2-[(2- O -(3-methylbutanoyl)-3,4-di- O -sulfo- β - D -glucopyranosyl]oxy]kaur-16-ene-18,19-dioic acid) is reported in pink sticks representation. Suramin is reported in salmon sticks representation. Chebulinic acid is reported in white sticks representation. Some interactions below 5 Å are highlighted by dashed lines.

potentially different from the proposed substrate binding region. From our kinetics estimations on the AAC2 recombinant protein, we cannot exclude that BKA could bind either the complex AAC2-ATP or the complex AAC2-ADP from the matrix side (after ATP enters the carrier cavity from the matrix side or after ADP enters AAC2 carrier cavity from the cytosolic side). We also cannot exclude that BKA binds the empty AAC2 before it binds ATP or ADP during ADP/ATP exchange, without altering AAC2 K_m for ADP or ATP.

4.1.1. Effects of the newly identified high affinity ligands on AAC2 activity

In order to identify new highly selective AAC2 inhibitors, we performed a virtual screening of a chemical library and we predicted and successfully identified two new highly selective AAC2 competitive inhibitors, namely chebulinic acid and suramin, bioactive in the μM /sub- μM range, as ascertained through in vitro transport assays on the human recombinant AAC2. We observed that suramin (a synthetic sulfonated naphthylamine [75]) has $K_i = 0.3 \mu\text{M}$, whereas chebulinic acid (an ellagitannin found in the seeds of *Euphoria longana* or *Terminalia chebula* [76]) has $K_i = 2.1 \mu\text{M}$. It was also verified that chebulinic acid and suramin are further selective for AAC2 given that human ORC1 is not inhibited at all by both the newly proposed inhibitors, whereas human AGC1 and APC1 are further weakly inhibited (maximal residual activity around 40%). AGC1 and APC1 are better inhibited than ORC1, in particular by suramin, although considering that AGC1 translocates acidic amino acids, at variance with APC1 that translocates adenine nucleotide derivatives (i.e. ATP-Mg). Notably, chebulinic acid and suramin concentrations used for estimating their ability in inhibiting other mitochondrial carriers is $10 \mu\text{M}$ (Fig. 8) that is a concentration about 5–25 times higher than the estimated K_i of both inhibitors for AAC2.

4.2. Selectivity of the analysed inhibitors in the context of amino acid composition of the different investigated mitochondrial carrier binding regions

We retain that the ability of suramin in inhibiting AAC2 better than chebulinic acid can be ascribed to its six sulfonic functional groups that bind basic (R80, R188, R280, K23) and hydrophilic residues (N88, Q89, Y187) located in the top half of AAC2 carrier cavity. Also CATR shows two sulfonic groups involved in the binding of the same basic/hydrophilic residues in the crystallized BtAAC1-CATR complex [24] (Fig. 9 and Table 3). The same residues are also involved in the binding of hydroxyl and carbonyl groups of chebulinic acid. It is also shown that suramin and chebulinic acid (both bigger than CATR) occupy the same area occupied by CATR in the BtAAC1-CATR crystallized complex (Fig. 9). Suramin and chebulinic acid appear to interact with the same AAC2 carrier cavity residues (including basic residues at the level of the matrix gate, Table 3) supposed to be involved in the binding of ADP, thus it is expected that they inhibit AAC2 entering the carrier cavity from the cytosolic face similarly to what observed with CATR [24,77]. The crucial role played by basic/hydrophilic residues of the AAC2 carrier cavity in the binding of the discussed inhibitors reflects the key role played by the same residues [44] in binding with higher affinity tri- and di-phosphate adenine nucleotides along substrate translocation.

Considering other mitochondrial carrier family members, APC1, AGC1 and ORC1 share with AAC2 the 30%, 29% and 22% of identical amino acids, respectively. Despite of the low percentage of identical amino acids, MCs share a similar overall architecture and exhibit a tripartite structure consisting of three tandemly repeated homologous domains of about 100 amino acids in length. They also have a similarly located common substrate binding,

Table 3

Residues within 4 Å from the discussed inhibitors.

Residues involved in the binding of the 3 inhibitors are listed in the table. Residues within 3 Å from the discussed inhibitors are reported in bold characters. The reported residues belong to the six transmembrane (TM) helices and face the carrier cavity from the cytosolic gate to the matrix gate.

	AAC2 residues		
	CATR	Suramin	Chebulinic acid
TM Helix 1		Ala19 Ser22	Ser22
	Lys23	Lys23 Glu30 Lys33	Lys23
TM Helix 2	Arg80 Thr84 Gln85 Asn88 Lys92	Arg80 Thr84 Gln85 Asn88	Arg80 Thr84 Gln85 Asn88
TM Helix 3	Gly124 Ser127 Leu128 Val131 Asp135 Val179	Gly124 Leu128	Gly120 Gly124 Leu128 Asp135
TM Helix 4	Ser180 Gly183 Ile184 Tyr187 Arg188	Ser180 Gly183 Ile184 Tyr187 Arg188	Ser180 Gly183 Ile184 Tyr187 Arg188
TM Helix 5	Ser228 Phe231 Asp232 Arg235 Arg236	 Asp232 Arg235 Arg236	Thr221 Gly225 Ser228 Tyr229 Asp232 Arg235 Arg236
TM Helix 6	Arg280	Asn277 Arg280 Gly281 Leu288	Arg280 Gly284 Leu288

approximately in the middle of the carrier cavity [44,78,79]. This binding site is open alternatively to the two opposite sides of the membrane, according to the translocation “single-binding center-gating pore mechanism” [77,79]. The binding of the substrate on one side induces conformational changes in the carrier that reorient the binding site to the opposite side determining the conversion of the c-conformation (open towards the cytosol) into the m-conformation (open towards the matrix) [77,79] and vice versa. It is worth noting that it has recently been shown that MCs can be divided in subfamilies characterized not only by their substrate specificity but also by a specific set of amino acid triplets [1,44,79–81]. These triplets consist of the aligned symmetry-related amino acids of each carrier when their three repeat sequences are aligned [44,79,81] (Fig. 10). Notably, the complete set of characterizing triplets of the mitochondrial carrier subfamilies AGC, APC, AAC and ORC were defined [80] and the role/importance of characterizing triplets, in particular triplets 84, 85 and 88, in substrate translocation and conformational changes was explained [44]. By comparing the characterizing triplets of AAC2, AGC1, APC1 and ORC1 (Fig. 10) it is observed that AGC1 is the only one that shows a basic residue (K403) at triplet 85 where AAC2 shows an arginine (R188) residue (Fig. 10). ORC1 and APC1 show no charged residues at triplet 85. It is also observed that AGC1 and APC1 show a basic lysine residue (K406 and K268, respectively) at triplet 88 not shared by AAC2 and ORC1 (Fig. 10). Notably, AGC1, APC1 and ORC1 show a conserved acidic glutamate residue at triplet 84 (E402, E264 and E77, respectively) not shared by AAC2. Given the involvement of triplets 84, 85 and 88 in the

proposed mitochondrial carrier substrate binding area [44] we retain that the presence of a basic residue at triplets 85 of AGC1 (also in presence of a further basic residue at triplet 88, i.e. in APC1 and AGC1) can increase the specificity of ligands containing sulfonic groups versus specific mitochondrial carriers (i.e. AGC1 and at a lower extent APC1). The affinity of our inhibitors versus AGC1 and APC1 is lower than the affinity observed for AAC2, most likely due to the presence of acidic residues at triplet 84 (E264 in APC1 and E402 in AGC1), 81 (D491 in AGC1) and 88 (D361 in APC1) that make unstable the binding (due to repulsive interactions) of the negatively charged suramin and chebulinic acid within the substrate binding area of APC1 and AGC1. Notably, ORC1 is not sensible to suramin and chebulinic acid and this finding can be ascribed to the fact that ORC1 shows an acidic residue at triplet 84 (E77) and, beyond the basic residues at triplets 80 and 96, it shows no further basic residues in triplets protruding towards the top half carrier cavity (Fig. 10). These observations strengthen the hypothesis that these two inhibitors are highly selective for AAC2 among mitochondrial carrier family members.

4.3. Putative translational applications of CATR, BKA, suramin and chebulinic acid for the treatment of specific cancer types and other diseases

To the best of our knowledge the “traditional” AAC2 inhibitors, BKA and CATR, have not yet been deeply investigated from a pharmacological point of view. However, it is known that BKA has antiapoptotic properties [82], whereas CATR was identified as a molecule responsible of poisoning and necrosis events [26] and apoptosis triggering as a consequence of the opening of mitochondrial PTP [83].

We retain that BKA deserves to be tested as anti-apoptotic small-molecule for the treatment of mitochondrial rare diseases with increased apoptosis affecting specific tissues [84,85].

At variance with BKA, CATR should instead be tested as pro-apoptotic small-molecule in liver and kidney cancers, given that it spontaneously accumulates in liver and kidney in humans that ingested plants rich of CATR accidentally [29]. Notably, *in vitro* cytotoxicity and *in vivo* antitumor activity of *X. strumarium* extracts

(containing CATR) were assayed in transplantable tumours in mice with favourable results that we retain may be ascribed to AAC mediated apoptosis triggering [86].

Among the other described AAC inhibitors, suramin is a drug already approved by FDA with multiple pharmacological activities. In particular, suramin is a potent antagonist of P2Y2 receptors with IC50 values in the micromolar concentration range (about 50 μ M) [87]. Following our kinetic characterization (among the few performed on a recombinant protein) we can state that suramin is also a potent and selective inhibitor of the human AAC2.

Suramin was also employed in pre-clinical and clinical trials in which it was administered at a concentration lower than 20 μ M (considered as a non cytotoxic concentration [88]) but there are no data about AAC expression levels in tissues or cancer cell-lines from patients treated with suramin.

It is worth noting that, as a consequence of specific prostate and breast cancer clinical trials, suramin employment for treating those cancers was discontinued [89,90]. Nevertheless, it could be speculated that the effect of suramin on those clinical trials should be due largely to its interaction with purinergic receptors, whereas AAC-mediated mitochondrial apoptosis should represent a minor component of the action of suramin in the described trials, due to the presence of several interactors [87,88,90,91] that can limit mitochondrial targeting.

We retain that suramin (containing sulfonic groups like CATR) deserves to be tested in liver and kidney cancer showing dysregulated AACs, because it is expected to show the same properties of CATR, known to accumulate spontaneously in liver and kidney [29]. Notably, before starting new clinical trials with suramin, it could be useful to improve mitochondrial targeting for reaching a better result by triggering in a more specific way the AAC mediated mitochondrial apoptosis.

It should be noticed that suramin was also successfully used for the treatment of human african trypanosomiasis [91–93]. It appears that suramin administered to trypanosomiasis patient at low doses (in the micromolar range) was found concentrated to high levels (in the millimolar range) in those protista responsible of trypanosomiasis [92–94]. It was proposed that suramin was able to block ATP-synthesis in trypanosomes affecting mammalian tissues

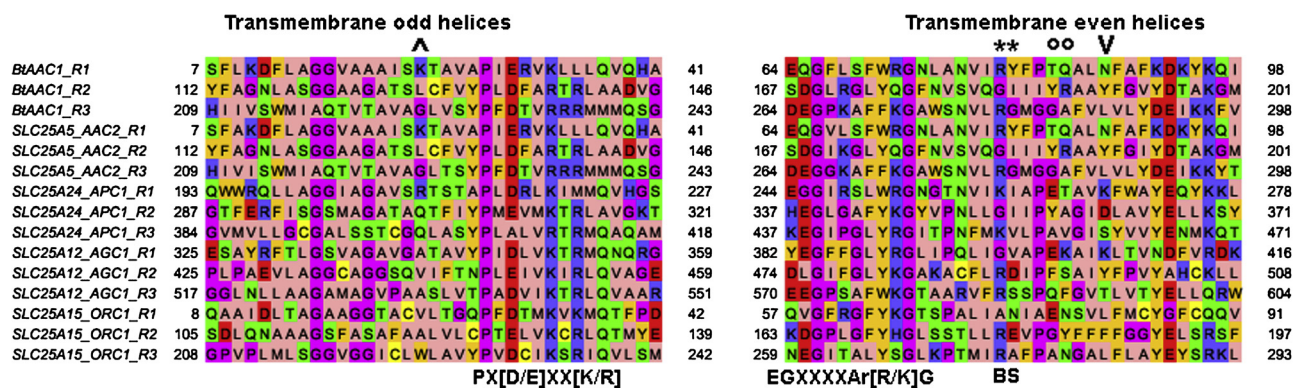


Fig. 10. Inter repeat sequence alignment of AAC2, APC1, AGC1 and ORC1.

Multiple sequence alignment of the three repeats (R1–3) of the investigated human MCs (SLC25A5_AAC2_R1-3, SLC25A24_APC1_R1-3, SLC25A12_AGC1_R1-3, SLC25A15_ORC1_R1-3) and of the three repeats of the bovine ADP/ATP carrier (BtAAC1_R1-3). For each carrier and each repeat (R1, R2, R3) only the odd transmembrane helices (H1, H3, H5) and the even transmembrane helices (H2, H4, H6) preceded by 10 amino acids are shown. Amino acids are colored according to the default Jalview Zappo style (<http://www.jalview.org/>). The labels PX[D/E]XX[K/R], EGXXXAr[R/K]G and BS indicate the position of the first part of the sequence motif, the second part of the sequence motif and the contact points of the proposed substrate binding site, respectively. The two asterisks “**” indicate the position of vertical triplets 80 and 81 (e.g. RGR and YIG, respectively in BtAAC1 and AAC2; KGK and IIV, respectively in APC1; GRR and VDS, respectively in AGC1; ARR and NEA, respectively in ORC1) forming the contact points of the mitochondrial carrier family common substrate binding site. The two circles “o” indicate vertical triplets 84 (consisting of residues TGY in BtAAC1 and AAC2; EYA in APC1; EFQ in AGC1; EGA in ORC1) and 85 (consisting of residues QRA in BtAAC1 and AAC2; TAV in APC1; KSF in AGC1 and NYN in ORC1). The “v” symbol indicates triplet 88 residues (consisting of NYL in BtAAC1 and AAC2; KDS in APC1; KYT in AGC1; LFL in ORC1). The “^” symbol indicates triplet 23 residues (consisting of residues KLG in BtAAC1 and AAC2; RQQ in APC1; AVA in AGC1; VAW in ORC1).

[91] and we can speculate that ATP-synthesis inhibition observed in the described experiments on rat liver mitochondria [91] depends on the inhibition of AACs. Furthermore, suramin was recently proposed as antibacterial [95] for the treatment of tuberculosis, being able to target Mycobacterium RecA protein with IC50 values in the submicromolar range. The ability of suramin in binding several targets [96] makes it a drug deserving to be still studied in greater detail.

Concerning chebulinic acid, some chebulinic acid analogues were studied for their antifungal/antibacterial/antiviral properties [76]. It was reported that the phenolics and more in general the crude extracts from *T. chebula* administered to several malignant human cell lines (including breast cancer cell lines (*i.e.* MCF-7), an osteosarcoma cell line (HOS-1) and a prostate cancer cell line (PC-3)) decreased cell viability, inhibited cell proliferation and induced cell death in a dose dependent manner [97,98]. To the best of our knowledge the mechanism of the observed cancer cell growth inhibition in those cell-lines has not yet been clarified. Based on our kinetic characterization we can speculate that a low concentration (less than 20 μ M) of chebulinic acid could be effective on tumors (similarly to what observed for suramin) by triggering AAC mediated mitochondrial apoptosis, without being cytotoxic for healthy tissues.

4.4. Delivery of AAC2 inhibitors to mitochondria of specific tissues

Early studies [99] proved that ATR at concentration as low as 20 μ M inhibited mitochondrial adenine nucleotide translocation, resulting in oxidative phosphorylation and Krebs cycle oxidative reactions blocking [29]. Similar observations were also made using bovin liver, kidney and heart [100]. Thus, we retain that the competitive AAC2 inhibitors, CATR (the ligand with the lowest K_i), suramin (already used in cancer therapy) and chebulinic acid deserve to be tested on the bench as “apoptosis inducers” in all those cancer types showing dysregulated AACs. It is worth noting the AAC-mediated mechanism of apoptosis-triggering depends on AAC ability to work as an apoptosis switcher in the context of the PTP opening [9]. Thus, we expect that CATR-like AAC inhibitors and more in general AAC-inhibitors able to bind AAC from the cytosolic side should be able to trigger apoptosis as a consequence of their binding to AACs, as long as AACs are expressed in affected tissues. It could even be speculated that cancers showing AAC down-regulated could need a lower amount of AAC inhibitors for triggering mitochondrial apoptosis (also according to [101]).

More in general, for improving mitochondrial targeting and using the lowest amount of the proposed toxic inhibitors, those inhibitors could be embedded within functionalized liposomes that are known to be able to target mitochondria efficiently [82].

However, the best way for reducing side-effects due to the indiscriminate cytotoxicity of the proposed inhibitors should be represented by their conjugation to antibodies directed against specific (or highly selective) plasma membrane receptors that could be internalized making specific the delivery of the proposed inhibitors to the affected tissues [102,103]. On this concern it is known that the indiscriminate cytotoxicity of other even more toxic ligands (*i.e.* the antibiotic calicheamicin) is avoided by conjugating it to antibodies [102,104].

5. Conclusions

Our computational strategy for identifying new AAC inhibitors was successful and we shall continue in screening other chemical libraries for searching new more specific AAC inhibitors to be tested on both the recombinant AAC2 protein and AAC2 dysregulated cancer cells. It should be stressed that CATR, BKA, suramin, chebulinic acid, STE and also melezitose and

saikosaponin (among the tested ligands) can be used as ligand templates to be modified by adding or modifying specific functional groups (*i.e.* by adding sulfonic groups) for drawing new highly specific AAC inhibitors to be tested *in vitro* and *in vivo* and to be delivered to mitochondria of cancer affected tissues, by using functionalized liposomes and/or antibody-conjugation, for triggering AAC mediated mitochondrial apoptosis. Furthermore, we can speculate that other AAC paralogs (in particular AAC1 and AAC3 showing different tissue expression patterns [10,13]) are expected to be protein targets of suramin and chebulinic acid due to the percentage of identical amino acids that AAC1 and AAC3 share with AAC2 (meanly more than 88%).

It is known that inhibitors of mitochondrial activity are already used in conventional therapy for the treatment of several cancers in combination with other chemotherapeutics to reduce drug resistance [105]. For this reason, we retain that it should be considered the possibility to target specific AACs within mitochondria of affected tissues with AAC inhibitors, in combination therapy with traditional cancer therapeutics, for triggering AAC mediated mitochondrial apoptosis, in those cancer affected tissues expressing functional AACs and/or showing dysregulated AACs.

Acknowledgements

Authors would like to thank the Italian Association for Cancer Research (AIRC—Associazione Italiana Ricerca sul Cancro, www.airc.it, grant number 12028 to C.L.P.) for having supported this project. The computational work has been executed in part on the IT resources made available by ReCaS, a project financed by the MIUR (Italian Ministry for Education, University and Research) in the “PON Ricerca e Competitività 2007–2013-Azione I-Interventi di rafforzamento strutturale” PONa3_00052, Avviso 254/Ric, in part on local computational resources available from the University of Bari (“Fondi ateneo” 2012). Authors would also like to thank the Italian Association for Mitochondrial Research (AIRM: www.mitoairm.it). Authors would also like to thank Dr. Veronica Stendardo and Dr. Angela Sarcina for technical assistance. Authors thank Prof. Ferdinando Palmieri for his invaluable teachings. The publication of this manuscript was approved by all the authors.

References

- [1] F. Palmieri, C.L. Pierri, Mitochondrial metabolite transport, *Essays Biochem.* 47 (2010) 37–52.
- [2] F. Palmieri, The mitochondrial transporter family (SLC25): physiological and pathological implications, *Pflug. Arch.* 447 (2004) 689–709.
- [3] F. Palmieri, The mitochondrial transporter family SLC25: identification, properties and physiopathology, *Mol. Asp. Med.* 34 (2013) 465–484.
- [4] M. Klingenberg, A.D.P. The, and ATP transport in mitochondria and its carrier, *Biochim. Biophys. Acta* 1778 (2008) 1978–2021.
- [5] P. Oliveira, K. Wallace, Depletion of adenine nucleotide translocator protein in heart mitochondria from doxorubicin-treated rats—relevance for mitochondrial dysfunction, *Toxicology* 220 (2006) 160–168.
- [6] J. Vandewalle, M. Bauters, E. Van, H. sch, S. Belet, J. Verbeeck, N. Fieremans, et al., The mitochondrial solute carrier SLC25A5 at Xq24 is a novel candidate gene for non-syndromic intellectual disability, *Hum. Genet.* 132 (2013) 1177–1185.
- [7] M. Bauer, A. Schubert, O. Rocks, S. Grimm, Adenine nucleotide translocase-1, a component of the permeability transition pore, can dominantly induce apoptosis, *J. Cell Biol.* 147 (1999) 1493–1502.
- [8] M. Zamora, M. Granell, T. Mampel, O. Viñas, Adenine nucleotide translocase 3 (ANT3) overexpression induces apoptosis in cultured cells, *FEBS Lett.* 563 (2004) 155–160.
- [9] A.P. Halestrap, G.P. McStay, S.J. Clarke, The permeability transition pore complex: another view, *Biochimie* 84 (2002) 153–166.
- [10] A. Doerner, M. Pauschinger, A. Badorf, M. Noutsias, S. Giessen, K. Schulze, et al., Tissue-specific transcription pattern of the adenine nucleotide translocase isoforms in humans, *FEBS Lett.* 414 (1997) 258–262.
- [11] G. Stepien, A. Torroni, A. Chung, J. Hodge, D. Wallace, Differential expression of adenine nucleotide translocator isoforms in mammalian tissues and during muscle cell differentiation, *J. Biol. Chem.* 267 (1992) 14592–14597.

- [12] V. Dolce, P. Scarcia, D. Iacopetta, F. Palmieri, A fourth ADP/ATP carrier isoform in man: identification, bacterial expression, functional characterization and tissue distribution, *FEBS Lett.* 579 (2005) 633–637.
- [13] K. Luciakova, G. Kollarovic, P. Barath, B. Nelson, Growth-dependent repression of human adenine nucleotide translocator-2 (ANT2) transcription: evidence for the participation of Smad and Sp family proteins in the NF1-dependent repressor complex, *Biochem. J.* 412 (2008) 123–130.
- [14] M. Le Bras, A. Borgne-Sanchez, Z. Touat, O. El Dein, A. Deniaud, E. Maillier, et al., Chemosensitization by knockdown of adenine nucleotide translocase-2, *Cancer Res.* 66 (2006) 9143–9152.
- [15] H. Faure Vigny, A. Heddi, S. Giraud, D. Chautard, G. Stepien, Expression of oxidative phosphorylation genes in renal tumors and tumoral cell lines, *Mol. Carcinog.* 16 (1996) 165–172.
- [16] A. Chevrollier, D. Loiseau, F. Gautier, Y. Malthièry, G. Stepien, ANT2 expression under hypoxic conditions produces opposite cell-cycle behavior in 143B and HepG2 cancer cells, *Mol. Carcinog.* 42 (2005) 1–8.
- [17] A. Chevrollier, D. Loiseau, B. Chabi, G. Renier, O. Douay, Y. Malthièry, et al., ANT2 isoform required for cancer cell glycolysis, *J. Bioenerg. Biomembr.* 37 (2005) 307–317.
- [18] K. Luciakova, P. Barath, D. Poliakova, A. Persson, B. Nelson, Repression of the human adenine nucleotide translocase-2 gene in growth-arrested human diploid cells: the role of nuclear factor-1, *J. Biol. Chem.* 278 (2003) 30624–30633.
- [19] Y. Choi, H.W. Lee, J. Lee, Y.H. Jeon, The combination of ANT2 shRNA and hNIS radiiodine gene therapy increases CTL cytotoxic activity through the phenotypic modulation of cancer cells: combination treatment with ANT2 shRNA and I-131, *BMC Cancer* 13 (2013) 143.
- [20] D.H. Park, B.K. Jung, Y.S. Lee, J.Y. Jang, M.K. Kim, J.K. Lee, et al., Evaluation of in vivo antitumor effects of ANT2 shRNA delivered using PEI and ultrasound with microbubbles, *Gene Ther.* 22 (2015) 325–332.
- [21] A. Chevrollier, D. Loiseau, P. Reynier, G. Stepien, Adenine nucleotide translocase 2 is a key mitochondrial protein in cancer metabolism, *Biochim. Biophys. Acta* 1807 (2011) 562–567.
- [22] B.P. Stuart, R.J. Cole, H.S. Gosser, Cocklebur (*Xanthium strumarium*, L. var. *strumarium*) intoxication in swine: review and redefinition of the toxic principle, *Vet. Pathol.* 18 (1981) 368–383.
- [23] K. Matsumoto, M. Suyama, S. Fujita, T. Moriwaki, Y. Sato, Y. Aso, et al., Efficient total synthesis of bongkreic acid and apoptosis inhibitory activity of its analogues, *Chemistry* 21 (32) (2015) 11590–11602.
- [24] E. Pebay-Peyroula, C. Dahout-Gonzalez, R. Kahn, V. Trézéguet, G. Lauquin, G. Brandolin, Structure of mitochondrial ADP/ATP carrier in complex with carboxyatractyloside, *Nature* 426 (2003) 39–44.
- [25] M. Klingenberg, Transport catalysis, *Biochim. Biophys. Acta* 1757 (2006) 1229–1236.
- [26] M. Turgut, C. Alhan, M. Gürgöze, A. Kurt, Y. Doğan, M. Tekatli, et al., Carboxyatractyloside poisoning in humans, *Ann. Trop. Paediatr.* 25 (2005) 125–134.
- [27] C. Daniele, S. Dahamna, O. Firuzi, N. Sekfali, L. Saso, G. Mazzanti, *Atractylis gummifera* L. poisoning: an ethnopharmacological review, *J. Ethnopharmacol.* 97 (2005) 175–181.
- [28] M.J. Stewart, V. Steenkamp, The biochemistry and toxicity of atractyloside: a review, *Ther. Drug Monit.* 22 (2000) 641–649.
- [29] D. Obatomi, P. Bach, Biochemistry and toxicology of the diterpenoid glycoside atractyloside, *Food Chem. Toxicol.* 36 (1998) 335–346.
- [30] P.V. Vignais, E.D. Duee, P.M. Vignais, J. Huet, Effects of atractyligenin and its structural analogues on oxidative phosphorylation and on the translocation of adenine nucleotides in mitochondria, *Biochim. Biophys. Acta* 118 (1966) 465–483.
- [31] B. Scherer, K. Grebe, P. Riccio, M. Klingenberg, The new atractyloside type compound as a high affinity ligand to the adenine nucleotide carrier, *FEBS Lett.* 31 (1973) 15–19.
- [32] R. Krämer, M. Klingenberg, Reconstitution of adenine nucleotide transport from beef heart mitochondria, *Biochemistry* 18 (1979) 4209–4215.
- [33] F. Palmieri, M. Klingenberg, Direct methods for measuring metabolite transport and distribution in mitochondria, *Methods Enzymol.* 56 (1979) 279–301.
- [34] F. Palmieri, C. Indiveri, F. Bisaccia, V. Iacobazzi, Mitochondrial metabolite carrier proteins: purification, reconstitution, and transport studies, *Methods Enzymol.* 260 (1995) 349–369.
- [35] G. Fiermonte, J. Walker, F. Palmieri, Abundant bacterial expression and reconstitution of an intrinsic membrane-transport protein from bovine mitochondria, *Biochem. J.* 294 (Pt. 1) (1993) 293–299.
- [36] G. Giannuzzi, N. Lobefaro, E. Paradies, A. Vozza, G. Punzi, C.M. Marobbio, Overexpression in *E. coli* and purification of the *L. pneumophila* Lpp2981 protein, *Mol. Biotechnol.* 56 (2014) 157–165.
- [37] N. Di, M.A. oia, S. Todisco, A. Cirigliano, T. Rinaldi, G. Agrimi, V. Iacobazzi, et al., The human SLC25A33 and SLC25A36 genes of solute carrier family 25 encode two mitochondrial pyrimidine nucleotide transporters, *J. Biol. Chem.* 289 (2014) 33137–33148.
- [38] G. Fiermonte, E. Paradies, S. Todisco, C. Marobbio, F. Palmieri, A novel member of solute carrier family 25 (SLC25A42) is a transporter of coenzyme A and adenosine 3',5'-diphosphate in human mitochondria, *J. Biol. Chem.* 284 (2009) 18152–18159.
- [39] G. Agrimi, A. Russo, P. Scarcia, F. Palmieri, The human gene SLC25A17 encodes a peroxisomal transporter of coenzyme A, FAD and NAD⁺, *Biochem. J.* 443 (2012) 241–247.
- [40] S. Todisco, M.A. Di Noia, A. Castegna, F.M. Lasorsa, E. Paradies, F. Palmieri, The *Saccharomyces cerevisiae* gene YPR011c encodes a mitochondrial transporter of adenosine 5'-phosphosulfate and 3'-phospho-adenosine 5'-phosphosulfate, *Biochim. Biophys. Acta* 1837 (2014) 326–334.
- [41] Y. Cheng, W.H. Prusoff, Relationship between the inhibition constant (K₁) and the concentration of inhibitor which causes 50 per cent inhibition (I₅₀) of an enzymatic reaction, *Biochem. Pharmacol.* 22 (1973) 3099–3108.
- [42] P.J. Henderson, A linear equation that describes the steady-state kinetics of enzymes and subcellular particles interacting with tightly bound inhibitors, *Biochem. J.* 127 (1972) 321–333.
- [43] R. Sánchez, A. Sali, Comparative protein structure modeling: introduction and practical examples with modeller, *Methods Mol. Biol.* 143 (2000) 97–129.
- [44] C.L. Pierri, F. Palmieri, A. De Grassi, Single-nucleotide evolution quantifies the importance of each site along the structure of mitochondrial carriers, *Cell Mol. Life Sci.* 71 (2014) 349–364.
- [45] C.L. Pierri, G. Parisi, V. Porcelli, Computational approaches for protein function prediction: a combined strategy from multiple sequence alignment to molecular docking-based virtual screening, *Biochim. Biophys. Acta* 1804 (2010) 1695–1712.
- [46] K. Aoki, M. Kanehisa, Using the KEGG database resource, *Curr. Protoc. Bioinform.* (2005) Chapter 1: Unit 1.12.
- [47] L. Han, Y. Wang, S.H. Bryant, A survey of cross-target bioactivity results of small molecules in PubChem, *Bioinformatics* 25 (2009) 2251–2255.
- [48] N.M. O'Boyle, M. Banck, C.A. James, C. Morley, T. Vandermeersch, G.R. Hutchison, Open babel: an open chemical toolbox, *J. Cheminform.* 3 (2011) 33.
- [49] D. Lagorce, B.O. Villoutreix, M.A. Miteva, Three-dimensional structure generators of drug-like compounds: DG-AMMOS, an open-source package, *Exp. Opin. Drug Discov.* 6 (2011) 339–351.
- [50] G. Morris, M. Lim-Wilby, Molecular docking, *Methods Mol. Biol.* 443 (2008) 365–382.
- [51] S. Cosconati, S. Forli, A.L. Perryman, R. Harris, D.S. Goodsell, A.J. Olson, Virtual screening with AutoDock: theory and practice, *Exp. Opin. Drug Discov.* 5 (2010) 597–607.
- [52] J.F. Sanchez, B. Kauffmann, A. Grélard, C. Sanchez, V. Trézéguet, I. Huc, et al., Unambiguous structure of atractyloside and carboxyatractyloside, *Bioorg. Med. Chem. Lett.* 22 (2012) 2973–2975.
- [53] G. Morris, R. Huey, A. Olson, Using AutoDock for ligand–receptor docking, *Curr. Protoc. Bioinform.* (2008) Chapter 8: Unit 8.14.
- [54] C. Oshiro, I. Kuntz, J. Dixon, Flexible ligand docking using a genetic algorithm, *J. Comput. Aided Mol. Des.* 9 (1995) 113–130.
- [55] G. Fiermonte, V. Dolce, F. Palmieri, Expression in *E. coli*, functional characterization, and tissue distribution of isoforms A and B of the phosphate carrier from bovine mitochondria, *J. Biol. Chem.* 273 (1998) 22782–22787.
- [56] G. Agrimi, Ma Di Noia, C.M.T. Marobbio, G. Fiermonte, F.M. Lasorsa, F. Palmieri, Identification of the human mitochondrial S-adenosylmethionine transporter: bacterial expression, reconstitution, functional characterization and tissue distribution, *Biochem. J.* 379 (2004) 183–190.
- [57] R. Wibom, F. Lasorsa, V. Töhönen, M. Barbaro, F. Sterky, T. Kucinski, et al., AGC1 deficiency associated with global cerebral hypomyelination, *N. Engl. J. Med.* 361 (2009) 489–495.
- [58] C.M. Marobbio, G. Punzi, C.L. Pierri, L. Palmieri, R. Calvello, M.A. Panaro, et al., Pathogenic potential of SLC25A15 mutations assessed by transport assays and complementation of *Saccharomyces cerevisiae* ORT1 null mutant, *Mol. Genet. Metab.* 115 (1) (2015) 27–32.
- [59] G. Fiermonte, L. De, F. eonardis, S. Todisco, L. Palmieri, F. Lasorsa, F. Palmieri, Identification of the mitochondrial ATP-Mg/Pi transporter. Bacterial expression, reconstitution, functional characterization, and tissue distribution, *J. Biol. Chem.* 279 (2004) 30722–30730.
- [60] R.L. Barbour, S.H. Chan, Characterization of the kinetics and mechanism of the mitochondrial ADP-ATP carrier, *J. Biol. Chem.* 256 (1981) 1940–1948.
- [61] J. Mifsud, S. Ravaut, E.M. Krammer, C. Chipot, E.R. Kunji, E. Pebay-Peyroula, et al., The substrate specificity of the human ADP/ATP carrier AAC1, *Mol. Membr. Biol.* 30 (2013) 160–168.
- [62] E. Pfaff, M. Klingenberg, Adenine nucleotide translocation of mitochondria. I. Specificity and control, *Eur. J. Biochem.* 6 (1968) 66–79.
- [63] G.J. Lauquin, P.V. Vignais, Interaction of (³H) bongkreic acid with the mitochondrial adenine nucleotide translocator, *Biochemistry* 15 (1976) 2316–2322.
- [64] N. Brustovetsky, M. Tropschug, S. Heimpel, D. Heidkämper, M. Klingenberg, A large Ca²⁺-dependent channel formed by recombinant ADP/ATP carrier from *Neurospora crassa* resembles the mitochondrial permeability transition pore, *Biochemistry* 41 (2002) 11804–11811.
- [65] A. Lawen, Another piece of the puzzle of apoptotic cytochrome c release, *Mol. Microbiol.* 66 (2007) 553–556.
- [66] N. Zamzami, G. Kroemer, The mitochondrion in apoptosis: how Pandora's box opens, *Nat. Rev. Mol. Cell Biol.* 2 (2001) 67–71.
- [67] J.-Y. Jang, Y. Choi, Y.-K. Jeon, C.-W. Kim, Suppression of adenine nucleotide translocase-2 by vector-based siRNA in human breast cancer cells induces apoptosis and inhibits tumor growth in vitro and in vivo, *Breast Cancer Res.: BCR* 10 (2008) R11–R.
- [68] J.Y. Jang, Y.K. Jeon, C.E. Lee, C.W. Kim, ANT2 suppression by shRNA may be able to exert anticancer effects in HCC further by restoring SOCS1 expression, *Int. J. Oncol.* 42 (2013) 574–582.
- [69] J.Y. Jang, Y.S. Lee, Y.K. Jeon, K. Lee, J.J. Jang, C.W. Kim, ANT2 suppression by shRNA restores miR-636 expression, thereby downregulating Ras and

- inhibiting tumorigenesis of hepatocellular carcinoma, *Exp. Mol. Med.* 45 (2013) e3.
- [70] D. Park, J. Chiu, G.G. Perrone, P.J. Dilda, P.J. Hogg, The tumour metabolism inhibitors GSAO and PENAO react with cysteines 57 and 257 of mitochondrial adenine nucleotide translocase, *Cancer Cell Int.* 12 (2012) 11.
- [71] E. Pfaff, H.W. Heldt, M. Klingenberg, Adenine nucleotide translocation of mitochondria. Kinetics of the adenine nucleotide exchange, *Eur. J. Biochem.* 10 (1969) 484–493.
- [72] S. Paul, S. Sengupta, T.K. Bandyopadhyay, A. Bhattacharyya, Stevioside induced ROS-mediated apoptosis through mitochondrial pathway in human breast cancer cell line MCF-7, *Nutr. Cancer* 64 (2012) 1087–1094.
- [73] R.R. Catharino, L.S. Santos, On-line monitoring of stevioside sweetener hydrolysis to steviol in acidic aqueous solutions, *Food Chem.* 133 (2012) 1632–1635.
- [74] P.V. Vignais, P.M. Vignais, G. Defaye, Gummiferin, an inhibitor of the adenine-nucleotide translocation. Study of its binding properties to mitochondria, *FEBS Lett.* 17 (1971) 281–288.
- [75] J. Dressel, The discovery of germanin by oskar dressel and richard kothe, *J. Chem. Educ.* 38 (1961) 620.
- [76] A. Bag, S.K. Bhattacharyya, R.R. Chattopadhyay, The development of *Terminalia chebula* Retz. (Combretaceae) in clinical research, *Asian Pac. J. Trop. Biomed.* 3 (2013) 244–252.
- [77] M. Klingenberg, *The ADP/ATP Carrier in Mitochondrial Membranes*, Plenum Publishing Corp., New York/London, 1976.
- [78] A.J. Robinson, E.R.S. Kunji, Mitochondrial carriers in the cytoplasmic state have a common substrate binding site, *Proc. Natl. Acad. Sci. U. S. A.* 103 (2006) 2617–2622.
- [79] F. Palmieri, C.L. Pierri, Structure and function of mitochondrial carriers—role of the transmembrane helix P and G residues in the gating and transport mechanism, *FEBS Lett.* 584 (2010) 1931–1939.
- [80] F. Palmieri, C.L. Pierri, G. De, A. rassi, A. Nunes-Nesi, A.R. Fernie, Evolution, structure and function of mitochondrial carriers: a review with new insights, *Plant J.* 66 (2011) 161–181.
- [81] A.J. Robinson, C. Overy, E.R.S. Kunji, The mechanism of transport by mitochondrial carriers based on analysis of symmetry, *Proc. Natl. Acad. Sci. U. S. A.* 105 (2008) 17766–17771.
- [82] Y. Yamada, K. Nakamura, R. Furukawa, E. Kawamura, T. Moriwaki, K. Matsumoto, et al., Mitochondrial delivery of bongkreik acid using a MITO-Porter prevents the induction of apoptosis in human HeLa cells, *J. Pharm. Sci.* 102 (2013) 1008–1015.
- [83] L. Hernández-Esquivel, Z. Natalia-Pavón, C. azueta, N. García, F. Correa, E. Chávez, Protective action of tamoxifen on carboxyatractyloside-induced mitochondrial permeability transition, *Life Sci.* 88 (2011) 681–687.
- [84] G. Di, S. Iovanni, M. Mirabella, A. D'Amico, P. Tonalì, S. Servidei, Apoptotic features accompany acute quadriplegic myopathy, *Neurology* 55 (2000) 854–858.
- [85] M. Mirabella, S. Di Giovanni, G. Silvestri, P. Tonalì, S. Servidei, Apoptosis in mitochondrial encephalomyopathies with mitochondrial DNA mutations: a potential pathogenic mechanism, *Brain* 123 (Pt. 1) (2000) 93–104.
- [86] J.M. Aranjani, A. Manuel, C. Mallikarjuna Rao, N. Udupa, J.V. Rao, A.M. Joy, et al., Preliminary evaluation of in vitro cytotoxicity and in vivo antitumor activity of *Xanthium strumarium* in transplantable tumors in mice, *Am. J. Chin. Med.* 41 (2013) 145–162.
- [87] M. Kaulich, F. Streicher, R. Mayer, I. Müller, C.E. Müller, Flavonoids—novel lead compounds for the development of P2Y2 receptor antagonists, *Drug Dev. Res.* 59 (2003) 72–81.
- [88] Y. Gan, J. Lu, B.Z. Yeung, C.T. Cottage, M.G. Wientjes, J.L. Au, Pharmacodynamics of telomerase inhibition and telomere shortening by noncytotoxic suramin, *AAPS J.* 17 (2015) 268–276.
- [89] M.R. Mirza, E. Jakobsen, P. Pfeiffer, B. Lindebjerg-Clasen, J. Bergh, C. Rose, Suramin in non-small cell lung cancer and advanced breast cancer: two parallel phase II studies, *Acta Oncol.* 36 (1997) 171–174.
- [90] C.A. Stein, R.V. LaRocca, R. Thomas, N. McAtee, C.E. Myers, Suramin: an anticancer drug with a unique mechanism of action, *J. Clin. Oncol.* 7 (1989) 499–508.
- [91] N.B. Calcaterra, L.R. Vicario, O.A. Roveri, Inhibition by suramin of mitochondrial ATP synthesis, *Biochem. Pharmacol.* 37 (1988) 2521–2527.
- [92] C.J. Bacchi, Chemotherapy of human african trypanosomiasis, *Interdiscip. Perspect. Infect. Dis.* 2009 (2009) 195040.
- [93] R.C. Russell, D. Otranto, R.L. Wall, *The Encyclopedia of Medical and Veterinary Entomology*, CABI, 2013.
- [94] M.P. Barrett, D.W. Boykin, R. Brun, R.R. Tidwell, Human African trypanosomiasis: pharmacological re-engagement with a neglected disease, *Br. J. Pharmacol.* 152 (2007) 1155–1171.
- [95] A. Nautiyal, K.N. Patil, K. Muniyappa, Suramin is a potent and selective inhibitor of *Mycobacterium tuberculosis* RecA protein and the SOS response: RecA as a potential target for antibacterial drug discovery, *J. Antimicrob. Chemother.* 69 (2014) 1834–1843.
- [96] N.H. Nam, K. Parang, Current targets for anticancer drug discovery, *Curr. Drug Targets* 4 (2003) 159–179.
- [97] A. Saleem, M. Husheem, P. Härkönen, K. Pihlaja, Inhibition of cancer cell growth by crude extract and the phenolics of *Terminalia chebula* retz. fruit, *J. Ethnopharmacol.* 81 (2002) 327–336.
- [98] Z.C. Yi, Y.Z. Liu, H.X. Li, Z. Wang, Chebulinic acid and tellimagrandin I inhibit DNA strand breaks by hydroquinone/Cu(II) and H₂O₂/Cu(II), but potentiate DNA strand breaks by H₂O₂/Fe(II), *Toxicol. In Vitro* 23 (2009) 667–673.
- [99] P. Vignais, P. Vignais, G. Defaye, Structure–activity relationship of atractyloside and diterpenoid derivatives on oxidative phosphorylation and adenine nucleotide translocation in mitochondria, *Atractyloside: Chem. Biochem. Toxicol.* 39 (1978) .
- [100] M. Klingenberg, The ADP and ATP translocator in mitochondria with particular attention to the effects of the atractylates, *Atractyloside: Chem. Biochem. Toxicol.* (1978) 69–107 Piccin Padova.
- [101] A.P. Halestrap, Mitochondrial permeability: dual role for the ADP/ATP translocator? *Nature* 430 (2004) 1 p following 983.
- [102] Y. Singh, M. Palombo, P. Sinko, Recent trends in targeted anticancer prodrug and conjugate design, *Curr. Med. Chem.* 15 (2008) 1802–1826.
- [103] T. Allen, Ligand-targeted therapeutics in anticancer therapy, *Nat. Rev. Cancer* 2 (2002) 750–763.
- [104] P.J. Carter, P.D. Senter, Antibody–drug conjugates for cancer therapy, *Cancer J.* 14 (2008) 154–169.
- [105] P. Marchetti, P. Guerreschi, L. Mortier, J. Kluzka, Integration of Mitochondrial targeting for molecular cancer, *Int. J. Cell Biol.* (2015) <http://www.hindawi.com/journals/ijcb/aip/> <http://www.hindawi.com/journals/ijcb/aip/283145/>.